Epigenetic therapy suppresses endocrine-resistant breast tumour growth by re-wiring ER-mediated 3D chromatin interactions

Authors

Joanna Achinger-Kawecka[1,2,9], Clare Stirzaker[1,2,9], Kee-Ming Chia[3], Neil Portman[2,3], Elyssa Campbell[1], Qian Du[1,2], Geraldine Laven-Law[4], Shalima S. Nair[1], Aliza Yong[3], Ashleigh Wilkinson[3], Samuel Clifton[1], Heloisa H. Milioli[2,3], Anthony Schmitt[5], Emily S. Wong[6,7], Theresa E. Hickey[4], Elgene Lim[2,3], Susan J. Clark[1,2,8]

[1]Epigenetics Research Laboratory, Genomics and Epigenetics Theme, The Garvan Institute of Medical Research, Sydney, New South Wales, Australia

[2]St Vincent's Clinical School, UNSW Sydney, New South Wales, Australia

[3]Connie Johnson Breast Cancer Research Laboratory, The Garvan Institute of Medical Research, Sydney, New South Wales, Australia

[4]Dame Roma Mitchell Cancer Research Laboratories, Adelaide Medical School, University of Adelaide, Adelaide, South Australia, Australia

[5]Arima Genomics, Inc., San Diego, California, USA

[6]Victor Chang Cardiac Institute, Sydney, New South Wales, Australia

[7]School of Biotechnology and Biomolecular Sciences, UNSW Sydney, New South Wales, Australia

[8]Lead Contact

[9]These authors contributed equally

Correspondence

s.clark@garvan.org.au (S.J.C.)

One line summary: Epigenetic therapy suppresses tumour growth in metastatic ER+ breast cancer *via* DNA hypomethylation-induced rewiring of long-range ER-mediated enhancer-promoter chromatin interactions to activate ER target genes involved in repression of proliferation and the cell cycle.

Keywords

3D genome architecture; DNA methylation; Decitabine, Hi-C; epigenetic therapy; ER+ breast cancer; endocrine-resistance; transcription factors; enhancers

Abstract

Three-dimensional (3D) epigenome remodelling is emerging as an important mechanism of gene deregulation in cancer. However, its potential as a target to overcome cancer therapy resistance remains largely unaddressed.

Here we show that treatment of endocrine-resistant estrogen receptor positive (ER+) breast cancer with an FDA-approved epigenetic therapy Decitabine (5-Aza-mC), results in genome-wide DNA hypomethylation and suppression of tumour growth in preclinical metastatic ER+ breast tumour xenograft models. Systematic integration of matched chromatin conformation capture (Hi-C), Promoter Capture Hi-C, RNA-seq and ER ChIP-seq data revealed widespread effects on epigenome deregulation, including de-compaction of higher order chromatin structure and loss of topologically associating domains (TAD) boundary insulation. Key enhancer ER binding sites were demethylated and re-activated after Decitabine treatment, resulting in new ER-mediated enhancer-promoter interactions and concordant activation of tumour-suppressive gene pathways. Importantly, we show that the activated ER target genes were also predictive of good outcome in multiple ER+ breast cancer clinical cohorts.

Together our study reveals a previously undescribed mechanism of Decitabine in re-wiring DNA methylation-dependent 3D genome architecture resulting in suppression of tumour growth, and highlights the potential of epigenetic therapy in targeting ER+ endocrine-resistant breast cancer.

55 **Main**

56 Around 70% of breast cancers are driven by the Estrogen Receptor-alpha (ER). ER is
57 a critical ligand-activated transcription factor that controls breast cancer cell
58 proliferation and tumour growth upon exposure to estrogenic hormones[1]. Drugs that
59 target ER pathways are highly effective in the treatment of ER+ breast cancer[2,3],
60 however *de novo* or acquired resistance to these agents (endocrine resistance) affects
61 a large proportion (>30%) of patients and is the major cause of breast cancer
62 mortality. Therefore, it is critical to understand mechanisms associated with endocrine
63 resistance to provide new therapeutic interventions that prevent or overcome the
64 resistant phenotype for ER+ breast cancer patients.

65

66 Genome-wide ER chromatin binding patterns, called cistromes, are associated with
67 ER-mediated transcriptional activity in endocrine-sensitive and endocrine-resistant
68 breast cancer contexts[1]. ER chromatin binding is primarily located at distal regulatory
69 elements and putative enhancer regions[4-8]. Previous studies carried out in endocrine-
70 resistant cell lines have demonstrated that differential ER binding is a key mechanism
71 that drives clinical response to endocrine therapies[4,9] and importantly, this endocrine
72 resistance can be characterised by epigenetic reprogramming of enhancer elements
73 occupied by ER in the endocrine sensitive state[10]. Epigenetic reprogramming involves
74 altered DNA methylation of enhancers that regulate ER-responsive genes and
75 represents a complementary mechanism that may drive primary and acquired
76 endocrine resistance. Enhancer hypermethylation associated with endocrine resistance
77 occludes ER recruitment, which results in transcriptional reprogramming of ER
78 signalling and estrogen independence[10].

79

80 Gene expression is highly regulated by (3D) genome architecture, from the local level
81 of chromatin compaction to the higher level organisation of topological associated
82 domains (TADs) and chromosome compartments[11]. Alterations to the 3D genome
83 architecture have been described in a number of different cancers, including prostate
84 cancer[12,13], breast cancer[14-18], gliomas[19], and several hematologic cancers[20,21].
85 Although cancer cells maintain the general pattern of 3D genome folding, distinctive
86 structural changes have been described in cancer genomes at all of levels of 3D
87 organisation[22]. We and others recently reported that 3D genome structure is also
88 disrupted in endocrine-resistant ER+ breast cancer cells[17,18,23], notably through long-

89 range chromatin changes at ER-enhancer binding sites that are DNA hypermethylated
90 in resistant cells[17]. These key findings suggest that DNA hypermethylation promotes
91 both reprogramming of the ER cistrome and 3D genome disorganisation, leading to
92 altered ER transcriptional activity in ER+ endocrine resistant breast cancer.
93
94 DNA demethylating agents such as Decitabine (5-aza-2'-deoxycytidine, DAC) have
95 emerged as a promising therapeutic strategy for treating various cancers[24]. Decitabine
96 is approved by many international regulatory agencies, including the US FDA and the
97 European Commission (EC), for treating haematological cancers[24]. In solid cancers
98 (including colorectal and ovarian cancer), Decitabine has been shown to demethylate
99 regulatory regions that result in re-activation of tumour suppressor genes[25,26].
100 Additionally, treatment with DNA de-methylating agents has been shown to stimulate
101 immune response pathways in cancer cells through increased transcription of DNA
102 repeat elements, which induces a viral mimicry response[27-29]. However, the direct
103 effect of these epigenetic drugs on the tumour cells, including epigenome and 3D
104 genome structure, remains largely unexplored, especially in clinically relevant
105 patient-derived model systems or clinical samples.
106
107 To test the therapeutic efficacy of epigenetic therapy with Decitabine in endocrine-
108 resistant ER+ patient-derived xenograft (PDX) models we assessed the molecular
109 consequences of treatment on DNA methylation, 3D genome architecture and
110 transcriptional pathways. Our data revealed that Decitabine treatment caused an
111 inhibition of endocrine-resistant tumour growth due to 3D epigenome remodelling
112 and re-activation of ER-driven tumour-suppressive gene pathways, highlighting the
113 potential of epigenetic therapy in treatment of ER+ endocrine-resistant breast cancer.

Results

Low-dose Decitabine inhibits tumour growth and decreases cell proliferation

To study the efficacy of epigenetic therapy in the context of endocrine-resistant ER+ breast cancer and to establish its impact on the 3D genome and epigenome, we used patient-derived xenograft (PDX) models (Gar15-13, HCI-005) (Fig. 1a). Gar15-13 and HCI-005 PDXs were derived from the metastases of two ER+ patients who had disease progression following one or more lines of endocrine therapy and have been used for several pre-clinical studies[30-34]. Using a low, well-tolerated and non-cytotoxic dose (0.5mg/kg; Extended Data Fig. 1a) of Decitabine, we first interrogated the anti-cancer effect of epigenetic therapy on tumour growth. Following tumour implantation and initial period of growth (to a volume of 150-200 mm^3), mice were randomized to twice-weekly injections of PBS (Vehicle) or 0.5mg/kg Decitabine. Treatment continued with twice-weekly measurement of tumour volume for 35 days or until tumour volume exceeded 1000 mm^3. At endpoint mice were sacrificed and tumour material collected for analysis. In both Gar15-13 and HCI-005 PDX models, Decitabine treatment elicited a strong growth inhibitory response (Fig. 1b, c) and a significant reduction in the proliferative index as measured by Ki-67 positivity at endpoint (Fig. 1d).

Decitabine induces widespread DNA hypomethylation

To directly identify the epigenetic reprogramming events induced by Decitabine treatment, we first analysed genome-wide DNA methylation data generated using Infinium EPIC Methylation arrays. EPIC arrays were performed on four biological replicates of Vehicle and Decitabine-treated PDX tumours at end-point. All Decitabine-treated tumours exhibited genome-wide DNA methylation loss (Fig. 1e, f and Extended Data Fig. 1b, c, P value < 0.0001, two-tailed Mann-Whitney test), with Gar15-13 showing more hypomethylation compared to HCI-005 (Fig. 1e and Extended Data Fig. 1d) (average 14.55% and 8.74%, respectively). To quantify the extent of DNA methylation loss, we identified differentially methylated probes (DMPs) and differentially methylated regions (DMRs) between Vehicle and Decitabine-treated tumours (Supplementary Table 1) and found that in Gar15-13, Decitabine treatment resulted in 279,908 hypomethylated DMPs, which were encompassed by 71,677 DMRs (total size >65Mb, mean size = 898.8, SD = 918.4).

148 Hypomethylated DMPs were mainly located at non-coding genomic regions (introns
149 and intergenic) (Extended Data Fig. 1e, f) and significantly enriched at putative
150 enhancer regions (Fig. 1g and Extended Data Fig. 1g) ($P < 0.001$, permutation test).
151 In agreement, we observed extensive DNA hypomethylation at enhancers in Gar15-13
152 tumours (approx. 21.58%; Extended Data Fig. 1h, P value < 0.0001, two-tailed Mann-
153 Whitney test), while promoters were less demethylated (approx. 10.12%; Extended
154 Data Fig. 1i, P value < 0.0001, two-tailed Mann-Whitney test).
155
156 We also evaluated genome-wide DNA methylation levels at different classes of
157 transposable elements (TEs) using the REMP package[35], including LTRs, LINE1
158 elements and Alu elements. We observed genome-wide loss of DNA methylation at
159 all repeat element sub-groups (Extended Data Fig. 1j and Extended Data Fig. 1k) with
160 ~12% loss of DNA methylation in Decitabine treated tumours. Additionally, we
161 observed TE expression alterations and activation of anti-viral signalling
162 (Supplementary Note), as previously observed with Decitabine treatment in other
163 cancers[27,28]. Notably, although all TE classes showed some degree of DNA
164 methylation loss, the extent of DNA hypomethylation measured at repeat elements
165 was less than those observed genome-wide and significantly less compared to DNA
166 hypomethylation at enhancer regions (Extended Data Fig. 1h).
167
168 **Decitabine-induced DNA hypomethylation reprograms the ER cistrome**
169 To examine the transcriptional consequences of Decitabine treatment in PDX tumours
170 (Gar15-13 and HCI-005), we next analysed RNA-seq data, followed by gene set
171 enrichment analysis (GSEA)[36] of differentially expressed genes. We found in the
172 ER+ endocrine-resistant PDX models that Decitabine treatment also negatively
173 correlated with gene signatures of cell proliferation and cell cycle (E2F targets, G2M
174 checkpoint and Myc targets; for example *SMC3*, *TK1* and *KIF20A*) (Extended Data
175 Fig. 2a, b), consistent with supressed tumour growth and decreased cytological
176 proliferation markers observed in both models. In Gar15-13 tumours, Decitabine
177 treatment also enriched for multiple hallmark genesets related to hormone signalling
178 (estrogen response early and late, androgen response) (Fig. 2a, Extended Data Fig.
179 2c). Notably, Decitabine treatment resulted in up-regulation of a large proportion of
180 genes belonging to the Hallmark Estrogen Response genesets (Extended Data Fig.

181 2d), including multiple co-regulators of ER (for example *CD44*, *PGR*, *KRT8* and
182 *KRT18*).
183
184 To further characterise the effect of Decitabine on estrogen signalling, we profiled ER
185 binding site (ERBS) patterns genome-wide in Vehicle (n = 4) and Decitabine-treated
186 Gar15-13 (n = 4) tumours via ER ChIP-seq. Differential binding analyses (Diffbind[4])
187 revealed reprogramming of the ER cistrome characterised by 1095 gained ERBS and
188 279 lost ERBS following Decitabine treatment as compared to Vehicle (FDR < 5%)
189 (Fig. 2b). Since FOXA1 is a critical ER pioneer factor required for ER to bind
190 DNA[37,38], we also assessed the FOXA1 cistrome and found stronger FOXA1 binding
191 at ERBS in Vehicle samples that were lost upon Decitabine treatment, while
192 Decitabine induced ERBS had weaker FOXA1 binding (Fig. 2b). We then mapped
193 the ER binding intensity at ERBS reprogrammed by Decitabine. As expected, gained
194 ERBS had a stronger average ER ChIP-seq signal in Decitabine samples as compared
195 to Vehicle, while lost sites showed a moderate decrease in binding intensity genome-
196 wide (Fig. 2c).
197
198 We next investigated the genomic distribution of gained and lost ER binding sites by
199 analysing the RefSeq annotation and ChromHMM state. Remarkably, over 75% of
200 gained ERBS were located at distal regions associated with active and poised
201 enhancers (Fig. 2d and Extended Data Fig. 2e), and these sites were enriched for the
202 estrogen response element (ERE) DNA motif (Fig. 2d). Lost ERBS were most
203 frequently positioned close to a TSS (> 40% less than 1Kb from TSS) (Extended Data
204 Fig. 2e), were associated with active promoters (Fig. 2e) and were enriched for Sp1
205 and NFY DNA response elements at promoter DNA motifs (Fig. 2e). Both lost and
206 gained ERBS were highly enriched for the FOXA1 motif.
207
208 Notably, we found that Decitabine-induced ERBS were significantly enriched for
209 ERBS found in endocrine-sensitive MCF7 cells (Extended Data Fig. 2f, h). This
210 suggests that Decitabine treatment of endocrine-resistant tumours may lead to
211 reprogramming of the ER cistrome toward an endocrine-sensitive ER binding pattern
212 of the primary tumour. To further elucidate this hypothesis, we interrogated ER ChIP-
213 seq data from two public clinical ER-ChIP-seq datasets of ER+ breast tumours. These
214 included 15 primary ER+ breast cancer patient tumours ((GSE32222)[4],

215 (GSE104399)[39] (see Methods)). We found that ER binding in primary tumours was
216 significantly enriched for Decitabine gained ERBS (*P* value < 0.001; permutation
217 test) and not enriched for Decitabine lost ERBS (Extended Data Fig. 2g, h).
218
219 Finally, we investigated whether the DNA hypomethylation observed with Decitabine
220 treatment was directly associated with reprogramming of the ER cistrome. We
221 examined the DNA methylation levels of EPIC probes overlapping gained and lost
222 ERBS. Gained ERBS showed an overall decrease (approx. 44.4%) in DNA
223 methylation (Fig. 2f and Extended Data Fig. 2i). Figure 2g shows a representative
224 example at the *ANKRD2* gene enhancer regions where a gain in ER binding in
225 Decitabine-treated tumours is associated with loss of DNA methylation (Fig. 2g). A
226 further example of the *BTBG9* gene locus is included in Extended Data Fig. 2j. In
227 contrast the small proportion of lost ERBS remained unmethylated in both Vehicle
228 and Decitabine treated samples (approx. 6.92%; Extended Data Fig. 2k), suggesting
229 that this subset of ERBS were lost independently of a direct change in DNA
230 methylation.
231
232 Together, these results indicate that Decitabine-induced DNA hypomethylation
233 stimulates expression of estrogen response genes *via* ER cistrome and subsequent
234 transcriptional reprograming as a putative mechanism of response.
235
236 **Loss of DNA methylation results in de-compaction of chromatin and alters TAD**
237 **boundary insulation**
238 Distinctive structural changes have been described in cancer genomes at all levels of
239 3D organisation[22]. We were therefore motivated to study if genome-wide DNA
240 hypomethylation induced by Decitabine may also lead to global changes in 3D
241 genome architecture. We analysed *in situ* Hi-C data corresponding to three biological
242 replicates of Vehicle and Decitabine-treated Gar15-13 PDX tumours (Supplementary
243 Note). First, to detect open (active) and closed (silent) genomic compartments (A and
244 B, respectively) we performed PCA analysis of the Hi-C data as described[40].
245 Comparison of eigenvalues between samples revealed differences between Vehicle
246 and Decitabine tumours as shown by reduced correlation (Extended Data Fig. 3a). To
247 further understand these differences, we directly compared the eigenvalues between
248 Vehicle and Decitabine-treated tumours and observed that while most bins retained

249 the same compartment status between the samples (either A to A or B to B), a large
250 number of bins became more A-type in Decitabine as compared to Vehicle (B to A
251 switch) (Fig. 3a). We next quantified this switching (see Methods) and identified 643
252 compartments (i.e. 2.28% of all compartments) that switched their assignment
253 between A and B (Extended Data Fig. 3b). Around 64% of the changes induced by
254 Decitabine involved compartment activation (B-type to A-type) (Fig. 3b). Notably,
255 we observed significant DNA hypomethylation at B to A switches, while A to B
256 switching regions maintained similar DNA methylation levels to Vehicle samples
257 (Fig. 3c). Furthermore, in agreement with B-compartments becoming more de-
258 methylated and active with Decitabine, we detected an overall increase in expression
259 of genes located at regions that switched their assignment from B to A in Decitabine-
260 treated tumours, while genes located at A to B switching compartments did not
261 significantly change expression (Extended Data Fig. 3c). The newly activated
262 compartments hosted 21 genes that decreased in expression and 87 genes that
263 increased in expression with Decitabine (Extended Data Fig. 3d, e). Furthermore, we
264 quantified A–A and B–B interaction frequencies in Decitabine and Vehicle-treated
265 tumours and found decreased interaction strength between closed compartments (B-B
266 interactions; $P = 0.025$, two-tailed Students t-test), increased contacts between active
267 compartments (A-A interactions; $P = 0.26$, two-tailed Students t-test) and increased
268 contacts between A-B compartments ($P = 0.011$, two-tailed Students t-test) (Fig. 3d,
269 e and Extended Data Fig. 3f, g).
270
271 Given that we observed DNA hypomethylation to be functionally associated with
272 changes to higher-order 3D genome organisation, we next investigated the impact of
273 Decitabine treatment on the organisation of topologically associated domains (TADs).
274 We observed a significant decrease in the average insulation score in Decitabine as
275 compared to Vehicle-treated tumours (~36.53 in Decitabine and ~46.74 in Vehicle)
276 (Fig. 3f and Extended Data Fig. 3h, P value < 0.0001, two-tailed Mann-Whitney test),
277 suggesting that loss of DNA methylation is associated with reduced segmentation into
278 TADs. Consistent with loss of TAD boundaries and potential merging of TADs, the
279 total number of TADs was decreased in Decitabine-treated samples (Fig. 3g) and their
280 corresponding average domain size increased (Extended Data Fig. 3i; $P = 0.0289$, t-
281 test). Analysis of differential TAD boundaries revealed a large percentage (43.2%) of
282 Vehicle-specific boundaries, which were lost in Decitabine tumours (Fig. 3h) and

283 characterised by decreased average insulation score in Decitabine tumours (Extended
284 Data Fig. 3j). We exemplify one such region, where a TAD was lost in Decitabine-
285 treated tumours, concomitant with loss of boundary insulation (Fig. 3i; further
286 examples in Extended Data Fig. 3k-l).
287
288 Together, these results indicate that DNA hypomethylation induced by Decitabine
289 treatment *in vivo* leads to significant de-compaction of chromatin, with reduced B-
290 type compartments, increased interactions within A-type compartments and
291 concomitant increase in regional gene expression. While most TADs maintain their
292 structure after Decitabine treatment, their boundaries become less insulated
293 suggesting increased intra-tumour heterogeneity in TAD structure and loss of some
294 TAD boundaries at the regions of chromosomal compartment de-compaction.
295
296 **Loss of DNA methylation rewires long-range promoter-anchored enhancer**
297 **interactions**
298 Since we observed that regulatory elements were significantly hypomethylated with
299 Decitabine treatment (Extended Data Fig. 1h), we next asked if there were alterations
300 in finer-scale 3D long-range interactions. To gain insights into chromatin interactions
301 at the level of individual promoters and enhancers, we investigated genome-wide
302 promoter-anchored contacts in three Decitabine and three Vehicle-treated tumours
303 using Promoter Capture Hi-C (PCHi-C) (Supplementary Note). Hi-C libraries were
304 hybridised to custom-designed genomic restriction fragments covering 23,711
305 annotated gene promoters, achieving a clear increase in the coverage of promoter-
306 anchored interactions as compared to Hi-C (Fig. 4a). To identify statistically
307 significant interactions between promoters and other regulatory elements from the
308 PCHi-C data, we used the CHiCAGO pipeline[41]. Promoter (bait) regions were
309 accordingly significantly enriched for active promoters, poised promoters and active
310 enhancers ChromHMM states in both Vehicle and Decitabine-treated tumours (Fig.
311 4b). Notably, putative enhancer other-end interacting regions (i.e. enhancer OEs;
312 exemplified in Fig. 4a) showed significant differential enrichment whereby active
313 promoters were preferentially enriched in Vehicle tumours and enhancers were
314 preferentially enriched in Decitabine-treated tumours, especially active enhancers
315 (Fig. 4b). This suggests that long-range interactions are rewired from promoter-
316 promoter to promoter-enhancer interaction after Decitabine treatment.

317 In order to directly identify differential promoter-anchored interactions, we integrated
318 the results generated using Chicdiff[42] pipeline with methods to intersect the promoter
319 bait and enhancer OE regions for each interaction (see Methods). In total, we found
320 13,088 stable (no change) and 4,111 dynamic (gained or lost) contacts for promoters
321 and 55,186 stable and 26,912 dynamic contacts for enhancer OEs (Fig. 4c). The
322 majority of promoter regions were common between the Decitabine and Vehicle
323 tumours. However, Decitabine treatment resulted in a large gain in the number of
324 dynamic enhancer OEs, while only a small number of enhancer OEs were lost (24,694
325 gained and 2,218 lost in Decitabine) (Fig. 4c). Notably, interactions at gained
326 enhancer OEs with Decitabine treatment were associated with longer interaction
327 distances as compared to these that were at maintained or lost (Fig. 4d), consistent
328 with an increased number of long-range interacting enhancers connecting to these
329 promoters.
330
331 We next compared the total number of unique promoter and enhancer OE regions
332 involved in interactions between Vehicle and Decitabine-treated tumours and found a
333 significant increase in the number of enhancer OEs in Decitabine tumours while the
334 number of interacting promoters stayed the same (Extended Data Fig. 4a, b). On
335 average we detected 3.73 unique enhancer OEs per promoter in Vehicle samples and
336 7.06 unique enhancer OEs per promoter in Decitabine samples (Fig. 4e). To directly
337 assess the gain in the number of interacting enhancers with Decitabine, we calculated
338 the number of interacting enhancer OEs per each individual promoter and compared
339 this number between Vehicle and Decitabine-treated tumours (Fig. 4f). We found that
340 the majority of bait promoters involved in interactions in Vehicle tumours showed a
341 large gain in the number of enhancer OEs they connect to in Decitabine-treated
342 tumours, suggesting reprogramming of one-to-many promoter-enhancer interactions.
343 Furthermore, we identified gained multi-way interactions that had, on average,
344 significantly higher CHiCAGO scores in Decitabine-treated tumours compared to
345 Vehicle (Wilcoxon P value < 0.0001) (Extended Data Fig. 4c), consistent with an
346 overall increase in the total number of interactions with Decitabine treatment.
347
348 To directly address if the identified gained enhancer-promoter interactions impact
349 regional transcription, we identified genes connected to newly gained enhancer OEs
350 and compared their average expression between Vehicle and Decitabine tumours. We

351 identified a total of 4025 genes associated with the new enhancer-promoter
352 interactions, of which 417 were upregulated after Decitabine treatment (*P* value <
353 0.05; logFC > 1) (Extended Data Fig. 4d). This suggests that the dynamic increase in
354 the number of enhancer OEs connected to a promoter results in an overall increase in
355 expression of genes and is in agreement with the current models of transcriptional
356 control *via* enhancer-promoter interactions[43,44].
357
358 Given that the frequency of interactions is directly linked with higher-order
359 compartment assignment, we next measured the overlap between dynamic promoter-
360 anchored interactions and A/B compartment flipping. A gain of interactions was
361 associated with a shift from B compartment assignment toward compartment A in
362 Decitabine-treated tumours (~76%) (Fig. 4g and Extended Data Fig. 4e), while a loss
363 of interactions was associated with switch from A-type to B-type assignment (~80%).
364 This was particularly pronounced at lost interactions involving promoter bait regions
365 (>90% switched A to B) (Fig. 4g).
366
367 Together, these results suggest that promoter interactions can be rewired following
368 DNA methylation loss associated with Decitabine treatment, leading to increased
369 promoter-anchored interactions involving multiple enhancers connecting to gene
370 promoters.
371
372 **Rewired promoter-anchored interactions regulate ER target genes**
373 In addition to 3D genome changes, our analyses revealed ER cistrome and
374 transcriptional reprogramming in tumour cells in response to Decitabine. To explore
375 the mechanistic role of rewired promoter-anchored interactions in the ER
376 transcriptional co-regulatory program, we evaluated whether specific transcription
377 factor motifs were related to gain in promoter-anchored interactions in Decitabine-
378 treated tumours. Dynamic promoter regions occurred at motifs associated with TSSs,
379 including El4 (ETS), NRF and Sp1 (Zf) (Extended Data Fig. 5a). Several TF binding
380 motifs were enriched at gained enhancer OEs, including CTCF, ERE, ELF5 and
381 ZNF165 (Fig. 5a). Consistent with motifs enriched at gained enhancer OEs, we found
382 significant enrichment for gained ER binding sites (Fig. 5b) and a genome-wide
383 increase in ER binding density at enhancer OEs induced by Decitabine treatment (Fig.

384 5c). We propose that these ER-associated promoter-enhancer interactions are
385 mediated by a change in ER binding at enhancer OEs ("ER-mediated interactions").
386
387 We next investigated gained ER-mediated promoter-enhancer interactions in detail by
388 identifying connected genes and comparing their expression between Vehicle and
389 Decitabine tumours. The majority (~74%) of genes involved in gained ER-mediated
390 interactions showed an overall increase in expression following Decitabine treatment
391 (Fig. 5d) and included established ER target genes (for example *KRT8*, *MYO3B,*
392 *SEMA3G*) as well as genes associated with a good clinical outcome in ER+ breast
393 cancer (for example *SPATA18, GALNT5, IGFBP4*). We examined one such
394 exemplary region (*SPATA18*), where multiple ER-mediated promoter-enhancer
395 interactions were gained with Decitabine treatment, concomitant with gain in ER
396 binding, loss of DNA methylation and activation of ER target genes (Extended Data
397 Fig. 5b). An ER binding site was gained following Decitabine treatment at the
398 enhancer region of the *SPATA18* gene, with multiple ER-mediated enhancer-promoter
399 interactions gained at this locus (Fig. 5e). Notably, this ERBS is also present in the
400 ER ChIP-seq data representing primary ER+ breast tumours from Ross-Innes *et al.*,
401 2012[4] and Severson *et al.*, 2018[39] as well as in the MCF7 ER+ breast cancer cell line
402 (Fig. 5e). Finally, we found that high expression of *SPATA18* gene is associated with
403 good prognosis in ER+ breast cancer (Extended Data Fig. 5c). We also examined two
404 additional regions at the *KRT8* (Fig. 5f and Extended Data Fig. 5e, f) and *MYOB3*
405 (Extended Data Fig. 5d) ER target genes, which exemplify the relationship between
406 Decitabine-induced gain of multiple ER-mediated enhancer-promoter interactions and
407 activation of ER target genes that are associated with good prognosis in ER+ breast
408 cancer. At both genes we found that ER binding sites gained with Decitabine
409 treatment were also present in primary ER+ breast tumours (Fig. 5f and Extended
410 Data Fig. 5d).
411
412 Next, we generated a gene signature by integrating RNA-seq, ER ChIP-seq, and
413 enhancer-promoter interactions. The resulting signature consisted of 17 genes that
414 were induced with Decitabine treatment (P value < 0.05 and logFC > 0) and located at
415 gained ER-mediated enhancer-promoter interactions (highlighted in bold in Fig. 5d).
416 We showed in the METABRIC and TCGA cohorts of ER+ breast cancer patients that
417 high expression of genes belonging to the signature was associated with better patient

418 prognosis and a higher proportion of luminal A tumour subtypes (Fig. 6a, b).
419 Accordingly, genes in the signature were expressed at higher levels in tumours from
420 patients with a better survival outcome (Fig. 6c, d). Taken together, these results
421 highlight the relationship between Decitabine-induced rewiring of ER-mediated
422 enhancer-promoter interactions and reveals candidate genes with prognostic potential
423 for good outcome and endocrine treatment response in ER+ breast cancer.
424
425 Our study provides extensive pre-clinical evidence that Decitabine treatment induced
426 DNA hypomethylation, which reprograms ER binding and rewires long-range 3D
427 enhancer-promoter interactions leads to re-expression of ER target genes (Fig. 6e).
428 Activated ER target genes are involved in repression of proliferation and cell cycle
429 genes, consistent with Decitabine-induced suppression of tumour growth and
430 significant anti-proliferative effect as assessed by Ki67 expression.
431
432 **Discussion**
433 Three-dimensional (3D) epigenome remodelling, including widespread changes to
434 DNA methylation and 3D chromatin structure, is an emerging mechanism of gene
435 deregulation in cancer. Our previous work demonstrated that DNA hypermethylation
436 and concomitant loss of ER binding at enhancers was a key event associated with
437 alterations in 3D chromatin interactions in ER+ endocrine-resistant breast cancer[45].
438 Therefore, we were intrigued to determine if these 3D chromatin alterations could be
439 switched with epigenetic therapies that induce DNA hypomethylation, leading to a
440 reversal of the endocrine resistant state and potentially associated with a beneficial
441 clinical outcome in ER+ breast cancer patients. To date, most studies investigating the
442 use of epigenetic therapies have focused on assessing efficacy in blood cancers and in
443 activating the immune system response. While some studies demonstrated that
444 Decitabine has anti-tumour properties in solid cancers (reviewed in [46]), the exact
445 mechanism that underpins this response was unclear and evidence for therapeutic
446 activity was not convincing[24,46].
447
448 Here, using patient-derived xenograft models of ER+ endocrine-resistant breast
449 cancer, we show that treatment with Decitabine induced DNA hypomethylation and
450 had potent anti-tumour activity *via* suppression of tumour growth and cell
451 proliferation gene pathways. To assess the broader genomic impact of DNA

452 hypomethylation, we analysed multiple layers of 3D genome organisation, including
453 chromosomal compartments, TADs and long-range promoter-enhancer chromatin
454 interactions and integrated the generated data with DNA methylation profiles,
455 transcriptome profiles and transcription factor (ER, FOXA1) cistrome profiles in
456 Decitabine and Vehicle-treated PDX tumours. Collectively we found that Decitabine
457 treatment results in enhancer DNA hypomethylation, reprogramming of ER
458 chromatin binding, rewiring of ER-mediated enhancer-promoter interactions, leading
459 to activation of tumour suppressive ER signalling pathways (Fig. 6e). Importantly,
460 rewired ER-mediated chromatin interactions connect enhancers to specific target
461 genes, which included ER target genes involved in cell cycle inhibition and tumor
462 suppressors that may directly inhibit tumor growth either in co-operation with or
463 independently of ER signalling. Such molecular mechanisms likely underpin the
464 Decitabine-induced tumour growth inhibition.
465
466 Decitabine has been previously demonstrated to have some therapeutic efficacy in
467 multiple subtypes of breast cancer and in overcoming drug resistance[47,48]. Transient
468 low-dose treatment with Decitabine resulted in decrease in promoter DNA
469 methylation, gene re-expression, and had antitumor effect *in vivo* in breast cancer
470 cells[49]. Low-dose Decitabine has also been shown to prevent cancer recurrence by
471 disrupting the pre-metastatic environment through its effect on myeloid-derived
472 suppressor cells in breast and other cancers[50]. In triple negative breast cancer (TNBC)
473 PDX organoids, Decitabine sensitivity was positively correlated with protein levels of
474 DNMTs, suggesting DNMT levels as potential biomarkers of response[51]. A recent
475 study of Decitabine in a panel of breast cancer cell lines observed that Decitabine also
476 induced genes within apoptosis, cell cycle, stress, and immune pathways[52]. However,
477 knockdown of key effectors of the immune pathway did not affect Decitabine
478 sensitivity suggesting that breast cancer growth suppression by Decitabine is
479 independent of viral mimicry.
480
481 We found that the low dose Decitabine treatment we used resulted in minimal DNA
482 hypomethylation at repetitive elements (Δ ~12%). Despite this, we observed a
483 relatively large number of TEs becoming activated with treatment, consistent with
484 previous studies in cancer cell lines[53]. Loss of DNA methylation at repetitive elements
485 and expression of TEs has been shown to drive viral mimicry response in tumours

486 treated with epigenetic therapies[27-29]. In agreement with studies in colorectal tumour
487 cells[27,54], our results indicate that treatment with Decitabine results in up-regulation of
488 multiple immune pathways (Interferon and Inflammatory Response pathways), which
489 could promote anti-tumour immunity. However, immunodeficient NOD-*scid IL2rγ*^{null}
490 (NSG) mice required for PDX experiments in our study largely lack mature immune
491 cells and therefore the potential immune response could not solely account for the
492 tumour inhibitory effects of Decitabine treatment observed in our study. This
493 highlights the need to study both the immune-based and tumour-based mechanisms
494 that underpin response to epigenetic therapies.
495
496 There have been limited studies to date on the role of DNA methylation in shaping the
497 3D genome organisation. Simultaneous profiling of DNA methylation and 3D
498 genome in single cells revealed pervasive interactions between these two epigenetic
499 layers in regulating gene expression[55]. Additionally, binding of CCCTC-binding
500 factor (CTCF), an insulator protein involved in creating chromatin loops and domain
501 boundaries has been shown to be methylation-sensitive[56-59]. DNA hypermethylation at
502 CTCF binding site in *IDH* mutant gliomas results in its reduced CTCF binding, loss
503 of insulation between topological domains and aberrant gene activation[19]. More
504 recently, DNA hypomethylation has been shown to result in de-compaction of
505 chromatin and loss of compartmental organisation[54,60,61]. This is consistent with our
506 data showing closed (B-type) to active (A-type) compartment shifting with
507 Decitabine-induced DNA hypomethylation and reduced interactions between B-type
508 compartments.
509
510 Importantly, no studies have examined the effect of epigenetic therapy and DNA
511 hypomethylation on ER-mediated chromatin interactions and transcriptional
512 programs. The ER chromatin binding profiles (cistromes) are distinct in breast
513 cancers that have poor versus favourable patient outcomes and the ER cistromes of
514 poor outcome tumours is more like endocrine resistant versus endocrine sensitive
515 breast cancer cell lines[4]. A number of studies have suggested an important role of
516 DNA methylation in altering ER binding at regulatory elements[10,62]. We have
517 previously shown that DNA methylation differences underpin differential ER binding
518 events associated with endocrine resistance [10]. Furthermore, recent studies
519 demonstrated that ER-mediated 3D chromatin interactions are altered in endocrine-

520 resistant cells[17,18]. In this study, our 3D genome analyses following Decitabine
521 treatment indicated that rewiring of enhancer-promoter interactions and ER binding
522 change coincidentally in response to Decitabine-induced DNA hypomethylation. The
523 investigation of transcriptomic datasets demonstrated a strong association between
524 gain in ER-mediated enhancer-promoter interactions and activation of connected ER
525 target genes. These results add to the current research, showing that enhancer
526 reprogramming through transcription factor binding or chromatin remodelling can
527 promote transcriptional programs that are associated with endocrine response in
528 breast cancer[63,64]. This suggests an important role of ER-mediated enhancer-promoter
529 interactions in controlling tumor growth during Decitabine treatment.
530
531 Our high-resolution promoter interactions data also revealed an increase in the
532 number of interacting enhancers connecting to gene promoters induced by Decitabine.
533 We hypothesise that the overall increase in enhancer connectivity results in creation
534 of active transcription hubs[44] or frequently interacting regions[65] at activated genes,
535 which will be investigated in future studies. This is in agreement with recent reports
536 of transcriptional activation occurring in non-membrane bound nuclear compartments
537 that harbour multiway enhancer-promoter interacting hubs[66] as well as additive effect
538 of multiway enhancer interactions on gene expression[67].
539
540 In summary, our work highlights a novel molecular mechanism of epigenetic
541 therapies in endocrine-resistant ER+ breast cancer. We provide mechanistic insights
542 into how Decitabine-induced 3D epigenome remodelling contributes to its tumour
543 suppressive properties and position these 3D changes as potential targets for the
544 treatment of endocrine-resistant ER+ breast cancer.

545 **Methods**

546

547 **Patient-derived xenograft (PDX) models of ER+ breast cancer**

548 All *in vivo* experiments, procedures and endpoints were approved by the Garvan
549 Institute of Medical Research Animal Ethics Committee (HREC #14/35, #15/25) and
550 performed at the Garvan Institute of Medical Research using standard techniques as
551 described previously [30,68] in accordance with relevant national and international
552 guidelines. The Gar15-13 model was generated in-house at the St Vincent's Hospital
553 under the Human Research Ethics protocol (HREC/16/SVH/29) and the HCI-005
554 model was developed by the Welm laboratory at the Huntsman Cancer Institute
555 (University of Utah)[68]. Gar15-13 was derived from a resected breast cancer liver
556 metastasis of ER-positive, PR-negative, HER2-negative metastatic breast cancer[31].
557 HCI-005 was derived from a pleural effusion of ER-positive (ERmutL536P), PR-
558 positive, HER2-positive metastatic breast cancer. Growth of HCI-005 was supported
559 by estrogen supplementation in the form of a 60 day 17-β-estradiol pellet implanted
560 simultaneously with the tumour chunks. Mice implanted with Gar15-13 did not
561 receive estrogen supplementation as this model does not require additional estrogen
562 for growth[31].

563

564 At surgery, 4 mm^3 sections of tumour tissue were implanted into the 4th inguinal
565 mammary gland of 6–8-week-old female NOD-*scid* IL2Rγ^{null} (NSG) mice, obtained
566 from Australian BioResources (Sydney, Australia). For HCI-005, tumour growth was
567 supported by implantation of an E2 pellet inserted subcutaneously via the incision site
568 before it was sealed with an Autoclip wound clip. When tumours became palpable,
569 tumour growth was assessed twice weekly by calliper measurement (using the
570 formula: $width^2 \times length/2$) and mice were randomised to treatment arms when
571 tumours reached 200 mm^3 using an online randomisation tool
572 (https://www.graphpad.com/quickcalcs/randomize1.cfm) (n = 6 - 8 mice per group for
573 therapeutic studies, exact numbers specified in figure legends).

574

575 **Pharmacological treatments**

576 The DNA methyltransferase inhibitor, Decitabine (5-Aza-2'-deoxycytidine: Sigma,
577 Cat #3656) was reconstituted in PBS and stored at -80°C.

578 Decitabine was administrated in 0.5mg/kg/mouse dose in PBS 100ul IP 2 times
579 weekly. Vehicle mice were treated with 100µl PBS IP. Mice were treated for 60 days
580 or until tumour volume reached 1000 mm^3. Upon reaching ethical or pre-defined
581 experimental endpoints, mice were euthanized, and the primary tumour collected.
582 After weighing, the tumour was cut into pieces that were allocated to be snap-frozen,
583 fixed overnight at 4°C in 10% neutral-buffered formalin, or embedded in cryo-
584 protective optimal cutting temperature (OCT) compound before being snap frozen.
585 Frozen samples were kept at -80°C. Formalin-fixed samples were sent to the Garvan
586 Institute Histology Core Facility for paraffin embedding. Tumour growth curves
587 were analysed in GraphPad Prism (GraphPad Software) by two-tailed, unpaired t-test.
588 Tumour mass at end-point was analysed by two-tailed Mann-Whitney t-test as per
589 figure legends unless otherwise specified.
590
591 **Immunohistochemistry (IHC) and quantification**
592 Tumour tissue was harvested and immediately fixed in 10% neutral buffered formalin
593 at 4°C overnight before dehydration and paraffin embedding. Antibodies used for
594 IHC were anti-ER (M7047, 1:300, Agilent) and anti-Ki67 (M7240, 1:400, Agilent).
595 Primary antibodies were detected using biotinylated IgG secondary antibodies
596 (Agilent, 1:400), using streptavidin-HRP (Agilent) for amplification of signal
597 followed by the addition of 3,3′-diaminobenzidine (Sigma) substrate. Images were
598 scanned using Leica Aperio Slide Scanner (Leica Biosystems) and analysed using
599 QuPath software to differentiate tumour tissue from stroma and necrosis, and to
600 quantify Ki-67 positivity in tumour tissue.
601
602 **Low input *in situ* Hi-C in snap-frozen PDX tumour samples**
603 Tumour tissue samples were flash frozen and pulverized in liquid nitrogen before
604 formaldehyde cross-linking in TC buffer. Hi-C was then conducted using the Arima-
605 HiC kit, according to the manufacturer's protocols (Cat. #A510008) with minor
606 modifications. Briefly, for each Hi-C reaction between ~100,000 - 500,000 cells were
607 cross-linked with 2% formaldehyde and nuclei were isolated by incubating cross-
608 linked cells in Lysis Buffer at 4°C for 30 minutes. The Arima kit uses two restriction
609 enzymes recognizing the following sequence motifs ^GATC and G^ANTC (N can be
610 either of the 4 genomic bases), which after ligation of DNA ends generates 4 possible
611 ligation junctions in the chimeric reads: GATC-GATC, GANT-GATC, GANT-

612 ANTC, GATC-ANTC. Hi-C libraries were prepared using the Swift Biosciences
613 Accel-NGS 2S Plus DNA Library Kit with a modified protocol provided by Arima
614 with 8 PCR cycles for library amplification as required. Hi-C libraries were
615 sequenced on Illumina HiSeq X10 in 150bp paired-end mode.
616
617 **Promoter Capture Hi-C**
618 To perform promoter Capture Hi-C (PCHi-C), we computationally designed RNA
619 probes that capture promoter regions of previously annotated human protein-coding
620 genes. Promoter Capture was performed as previously described[69-71]. First, to identify
621 promoter capture targets, 23,711 unique Ensembl annotated genes were extracted
622 from the GRCh38 gene annotation file in Ensembl database, version 95. These
623 compromised of protein-coding (18,741), antisense (84), lincRNA (170), miRNA
624 (1,878), snoRNA (938), snRNA (1,898) or multiple (2) transcripts. We then located
625 transcription start sites (TSS) of each gene and mapped the TSS coordinates to the in
626 silico digested genome (^GATC and G^ANTC) and extracted the restriction fragment
627 containing the TSS, as well as one restriction fragment upstream and one restriction
628 fragment downstream for each TSS. The final target list of TSS mapped to 3
629 consecutive restriction fragments. The average length of the 3 consecutive restriction
630 fragments for each TSS is 786bp and the median is 927bp, with a range of 54-4174bp.
631 Moreover, for the individual restriction fragments smaller than 700bp, all nucleotides
632 within these fragments are less than or equal to 350bp from the nearest cut site, and
633 therefore the entire restriction fragment was defined as a target region for subsequent
634 probe design. This scenario represents the vast majority of cases, because the mean
635 length of an individual restriction fragment is 263bp, with a median of 431bp.
636 However, if an individual restriction fragment was greater than 700bp, then the 350bp
637 on each inward facing edge of the restriction fragment was defined as a target region
638 for probe design, and the centre most portion of the restriction fragment was excluded
639 from the probe design. After this final processing, a final BED file of target bait
640 regions was input into the Agilent SureDesign tool, and probes were designed using a
641 1X tiling approach, with moderate repeat masking and balanced boosting. Promoter
642 Capture was carried out using Hi-C libraries from three Vehicle-treated tumour
643 samples and three Decitabine-treated tumour samples with the SureSelect target
644 enrichment system and RNA bait library according to manufacturer's instructions
645 (Agilent Technologies kit), using 12 post-capture PCR cycles as required. PCHi-C

646 libraries were sequenced on the Illumina HiSeq X10 platform in 150bp paired-end
647 mode.
648
649 **Microarray genome-wide DNA methylation**
650 DNA from four Decitabine and four Vehicle-treated tumours from two PDX models
651 (Gar15-13 and HCI-005) was isolated from snap-frozen tumour samples using the
652 Qiagen QIAamp DNA Mini Kit. DNA (500ng) was treated with sodium bisulphite
653 using EZ-96 DNA methylation kit (Zymo Research CA, USA). DNA methylation
654 was quantified using the Illumina InfiniumMethylationEPIC (EPIC) BeadChip
655 (Illumina, CA, USA) run on the HiScan System (Illumina, CA, USA) using
656 manufacturer's standard protocol.
657
658 **ChIP-seq**
659 Tumour samples were snap-frozen in Optimal Cutting Temperature compound
660 (Tissue-Tek) and used for ER and FOXA1 ChIP-seq experiments. Using a cryostat
661 (Leica, #CM3050-S), a minimum of 50 x 30 µm sections were cut from each tumour
662 at -20℃ and subjected to double cross-linking with DSG and formaldehyde as
663 previously described[33]. ER ChIP-seq was performed with an anti-ER antibody (Santa
664 Cruz, SC-543X) and FOXA1 ChIP-seq was performed with an anti-FOXA1 antibody
665 (Abcam, Ab23738). 5µg of antibody was used to ChIP each tumour sample and 10ng
666 of immunoprecipitated DNA was submitted to the David R. Gunn Genomics Facility
667 at the South Australian Health and Medical Research Institute (SAHMRI) for
668 sequencing. Conversion of the DNA into sequencing libraries was performed using
669 the Ultralow Input Library Kit (Qiagen, #180495) and sequenced on the Illumina
670 NextSeq 500 (Illumina) in 75bp single-end mode to achieve a minimum of 20 million
671 reads per sample.
672
673 **RNA-seq**
674 RNA was extracted from snap-frozen tumour PDX tissue samples using the RNeasy
675 Mini Kit (QIAGEN) and quality of purified RNA was confirmed with RNA
676 ScreenTape TapeStation (Agilent). All samples processed for RNA-seq had a RIN
677 equivalent (RIN^e) quality score ≥ 8.0. Total RNA was supplied to the genomics core
678 facility (Kinghorn Centre for Clinical Genomics) for library preparation and
679 sequencing. RNA was prepared for sequencing using the TruSeq Stranded mRNA

680 Library Prep kit (Illumina) and libraries were sequenced on Illumina NovaSeq 6000
681 S4 in paired-end mode.
682
683 **EPIC DNA methylation analyses**
684 Raw intensity data (IDAT) files were imported and quality controlled using *minfi*
685 package (v.1.34.0)[72]. Data was then normalised with background correction. To
686 reduce the risk of false discoveries, we removed probes affected for cross-
687 hybridization to multiple locations on the genome or overlapped SNPs, as previously
688 described[73]. Beta (β) values were calculated from unmethylated (U) and methylated
689 (M) signal [M/(U + M + 100)] and ranged from 0 to 1 (0 to 100% methylation). β
690 values of loci whose detection P values were > 0.01 were assigned NA in the output
691 file. To map EPIC arrays to hg38/GRCh38 assembly, all probes were annotated with
692 the EPIC.hg38.manifest.tsv.gz files as described in[74].
693 For initial visualisation of the EPIC data, multidimensional scaling plots were
694 generated using the 'mdsPlot' function in the *minfi* Bioconductor package
695 (v.1.34.0)[72]. Differential analyses were then performed between treatment arm with
696 Decitabine versus Vehicle samples. For each comparison, β values were transformed
697 using logit transformation: $M = \log2(\beta/(1-\beta))$. We used the limma package (v.3.46)[75]
698 to identify DMPs between sample groups with adjusted *P* value cut-off of < 0.01. The
699 R package DMRcate (v.2.2.3)[76] was used to identify DMRs, with DMP *P* value cut-
700 offs of FDR < 0.01. DMRs were defined as regions with a maximum of 1000
701 nucleotides between consecutive probes and a minimum of 2 CpG sites, a methylation
702 change > 30% and we applied Benjamini-Hochberg correction for multiple testing.
703 ChromHMM data downloaded from GEO (GSE73783) for tamoxifen-resistant
704 (TAMR) MCF7 cells was used to annotate DMPs to chromatin states.
705 REMP R package (v.1.14.0)[35] was used to assess genome-wide locus-specific DNA
706 methylation of repeat elements (LTR, LINE1 and Alu) from EPIC data with
707 IlluminaHumanMethylationEPICanno.ilm10b5.hg38 annotation (GitHub).
708
709 **Hi-C analyses**
710 Hi-C sequenced reads (150bp paired-end) were quality checked with FastQ Screen
711 v.0.14.1[77] for mouse host reads contamination. Reads were then processed with
712 Xenome (v.1.0.1)[78] as described in [79]. Remaining reads were aligned to the human
713 genome (hg38/GRCh38) using HiC-Pro[80] (v.2.11.4). Initially, to generate Hi-C

714 contact matrices, the aligned Hi-C reads were filtered and corrected using the ICE
715 "correction" algorithm[81] built into HiC-Pro, which corrects for the CNV-related
716 variability in the tumours[82]. Inter-chromosomal interactions were excluded from
717 further analyses to control for the effect of inter-chromosomal translocations in the
718 tumours. Contact matrices for 3D genome feature annotation and visualisation were
719 created and Knight-Ruiz (KR) normalized using Juicer tools[83] using contact matrices
720 in .hic format generated by hicpro2juciebox script in HiC-Pro as input (hic file
721 version 8). Hi-C matrices were visualised using JuiceBox[84] and WashU Epigenome
722 Browser[85]. We confirmed data quality by assessing the proportion of cis/trans
723 interactions and percentage of valid fragments for each library. Overall, we obtained
724 an average of 100 million unique, valid contacts per replicate (~310 million per
725 treatment arm), for an average resolution of 10kb. Statistics for each library can be
726 found in Supplemental Table 2. These data was used to derive loops, TAD boundaries
727 and chromosomal compartment structures.
728
729 **Insulation score and identification of TAD boundaries**
730 Topological domain boundary calling was performed by calculating insulation scores
731 in ICE normalised contact matrices at 20kb resolution using TADtool[86]. To identify
732 appropriate parameters, we called TADs across chromosome 1 using contact matrices
733 at 20kb and threshold values: 10, 50 and 100. The final TADs were called for all
734 chromosomes at window 102353 and cut-off value 50. Boundaries that were found
735 overlapping by at least 1 genomic bin were merged. Boundaries separated by at least
736 one genomic bin were considered different between datasets. Pyramid-like heatmap
737 plots were generated with GENOVA[87].
738
739 **Identification of compartments A and B**
740 For each chromosome in each sample, compartments where called using the standard
741 PCA method[40] in Homer package (version 4.8). The resolution was set to 50kb and
742 the window size to 100 kb. Compartments were defined as regions of continuous
743 positive or negative PC1 values using the findHiCCompartments.pl tool in Homer. To
744 detect which compartment is the open "A-type" and which is the closed "B-type," the
745 genome-wide gene density was calculated to assign the "A-type" and "B-type"
746 compartmentalisation. To identify genomic regions that switch between two
747 compartment types, we used correlation difference script (getHiCcorrDiff.pl) with

748 findHiCCompartments.pl tool in Homer. Compartments were considered common if
749 they had the same compartment definition within the same genomic bin.
750 Compartment changes between treatment arms were computed after considering
751 compartments that were overlapping between biological replicates, unless otherwise
752 indicated.
753 To directly quantify the tendency of each region to interact with the other regions in
754 either A or B compartments, we calculated the "A/B interaction ratio", defined for
755 each 100kb genomic window as the ratio of interaction frequency with A versus B
756 compartments using O/E matrix with GENOVA[87] (v1.0.0,
757 https://github.com/robinweide/GENOVA). Log_2 contact enrichments were plotted as
758 a heat saddle plot. Summarised A-A, B-B and B-A compartment strengths were
759 calculated as the mean log_2 contact enrichment between the top (A) or bottom (B)
760 20% of PC1 percentiles. The compartment strength ratio was calculated as log_2(A-
761 A/B-B).
762
763 **PCHi-C analyses**
764 PCHi-C sequenced reads were mapped and filtered using HiCUP (v.0.7.4)[88] with
765 hg38/GRCh38 genome digested with –arima flag and minimum di-tag length set to
766 20. Statistics for each library can be found in Supplementary Table 3. On target rate
767 was calculated by counting number of valid, unique reads overlapping bait fragments
768 (min. overlap > 0.6). Unique, valid mapped reads from HiCUP were converted into
769 .chinput files using bam2chicago.sh utility and obtained chinput files were further
770 filtered and processed with CHiCAGO (v.1.14.0)[41]. CHiCAGO design files were
771 created with following parameters to account for multiple restriction enzymes used in
772 the Arima HiC kit and the Arima-specific design of the bait fragments:
773 MaxLBrowndist = 75000; binsize = 1500; minFragLen = 25; maxFragLen = 1200.
774 Significant interactions were called with CHiCAGO using score cut-off of 5. All bait-
775 to-bait interactions were discarded. Chicdiff package[42] (v.0.6) was used to compare
776 PCHi-C data from Vehicle and Decitabine tumours and the difference in the mean
777 asinh-transformed CHiCAGO scores between conditions above 1 was used to
778 prioritise the potential differential promoter-anchored interactions. Only interactions
779 that have CHiCAGO score of more than 5 in at least 2 replicates were included for
780 downstream analysis. Volcano plots were generated using EnhancedVolcano R
781 package (v.1.8.0)[89]. For downstream analysis of merged replicate data and for

782 visualisation of interactions in WashU Epigenome Browser[85] replicates were merged
783 with CHiCAGO. We defined reprogrammed promoter-enhancer interactions by
784 constructing a consensus, gained and lost subset of promoter-anchors (baits) and other
785 end anchors (OEs) based on CHiCAGO promoter interactions, Chicdiff analysis and
786 setdiff R function across the replicates. The following criteria was used to obtain
787 these regions: CHiCAGO score > 5 in 2 out of 3 replicates in either condition,
788 Chicdiff generated asinh-transformed CHiCAGO scores between conditions above 1
789 and no overlap between regions, allowing for 10Kb maximal gap in 3 out of 3
790 replicates. ChromHMM data downloaded from GEO (GSE73783) for tamoxifen-
791 resistant (TAMR) MCF7 cells was used to annotate promoter-anchored interactions to
792 chromatin states.
793
794 **RNA-seq data analyses**
795 For canonical gene expression, RNA-seq raw reads were quality checked (FastQ
796 Screen v.0.14.1[77]). Sequence adaptors were trimmed using Trim Galore (v.0.11.2),
797 reads were processed with Xenome v.10.1.[78] to remove mouse sequences and
798 remaining reads were mapped with STAR (v.2.7.7a)[90] to the hg38/GRCh38 human
799 genome build with GENCODE v33 used as a reference transcriptome (parameter
800 settings: –quantMode TranscriptomeSAM–outFilterMatchNmin 101 –
801 outFilterMultimapNmax 20). Statistics for each library can be found in
802 Supplementary Table 4. TMM normalisation was applied to normalise for RNA
803 composition[91] and differential expression was performed with edgeR 3.18.1 [92] using
804 the generalised linear model (GLM). RNA-seq tracks were generated using bedtools
805 v.2.22 genomeCoverageBed to create normalised.bedGraph files and
806 bedGraphToBigWig (USCS utils) to create.bigwig files.
807 For analysis of TE expression, adapter-trimmed, human-only RNA-seq reads were
808 mapped with STAR (v.2.7.7a), allowing for multimapping alignments (flags: --
809 outFilterMultimapNmax 100 --outFilterMismatchNmax 100). Annotation GTF files
810 for canonical genes were downloaded from Ensembl genome browser (v.102,
811 GRCh38.p13 assembly) and TE annotation GTF file
812 (GRCm38_Ensembl_rmsk_TE.gtf) was downloaded from TEtranscripts [93] website
813 (http://hammelllab.labsites.cshl.edu/software/#TEtranscripts). Normalisation and
814 differential expression was performed for all genes and TEs using DESeq2[94]. TEs
815 with and FDR < 0.1 and logFC > 0.7 were considered differentially expressed in pair-

816 wise comparisons. Volcano plots were generated using EnhancedVolcano R package
817 (v.1.8.0)[89].
818
819 **ChIP-seq data analyses**
820 ChIP-seq reads were aligned against human genome (hg38/GRCh38) using bowtie2
821 with default parameters[95]. Non-uniquely mapped, low quality (MAPQ < 15) and PCR
822 duplicate reads were removed. Peak calling of individual ChIP–seq experiments was
823 performed with MACS2 with default parameters[96,97]. Statistics for each library can be
824 found in Supplementary Table 5. Consensus peaks were identified by intersecting
825 MACS2 peaks obtained from each sample using bedtools intersect (v.2.25.0) with
826 min. overlap > 0.6. Differential binding analyses were performed using DiffBind
827 (v.3.0.9)[4] and DESeq2 (v.1.3.0)[94] with FDR < 5%. Enrichment analyses were
828 performed using GAT[98], ChIPseeker (v.1.26.0)[99] and normalised to library size.
829 Merged bigwig tracks for visualisation were created from merged bam files from all
830 replicates using the bamCoverage function with scaling factor normalisation and
831 heatmaps and average profiles were plotted with deepTools2[100]. ChromHMM data
832 downloaded from GEO (GSE73783) for tamoxifen-resistant (TAMR) MCF7 cells
833 was used to annotate ER binding sites to chromatin states. The Homer motif
834 discovery suite[101] was used for motif analysis using the bed regions from differential
835 peaks detected by DiffBind with default parameters, using random, matched regions
836 as background. ER ChIP-seq data from primary breast tumours were obtained from
837 GSE32222[4] and GSE104399[39], and re-processed as described above. Merged bigwig
838 tracks for visualisation were created from merged bam files from all replicates using
839 the bamCoverage function with scaling factor normalisation and heatmaps and
840 average profiles were plotted with deepTools2[100].
841
842 **Gene ontology analysis**
843 Gene ontology enrichment analysis and pathway enrichment were done using GSEA
844 (v.4.1.0) and MSigDB 7.2[36]. All significant biological processes and pathways had an
845 adj. P value < 0.001.
846
847 **Clinical samples and survival analyses**
848 We used the METABRIC (Molecular Taxonomy of Breast Cancer International
849 Consortium)[102,103] dataset and the TCGA (The Cancer Genome Atlas) dataset [104,105]

850 for patient survival analysis. These datasets contain RNA-seq and microarray data as
851 well as detailed clinical information from breast cancer patients. Data was accessed
852 using cBioPortal (https://www.cbioportal.org/)[106]. Patient survival analysis was
853 performed using the survminer (v.0.4.9) R package. Survival curves were drawn using
854 ggplot2. Cohorts were split by mean gene expression and disease-specific survival
855 was compared by Cox proportional hazards analysis.
856
857 **Statistical analyses**
858 The Mann-Whitney-Wilcoxon test was used for 2-group non-parametric comparisons.
859 Unless otherwise stated, statistical tests were two-sided. Permutation test was used to
860 calculate empirical *P* values, which does not make any assumptions on the underlying
861 distribution of the data. Tumor growth curve data was analysed at ethical end point
862 using a two-tailed unpaired Student's *t*-test. IHC data were analysed by a two-tailed,
863 unpaired Student's *t*-test.
864
865 **Public datasets**
866 ChIP-seq data sets were downloaded from GSE32222 by Ross-Innes *et al.,* 2012[4] and
867 GSE104399 by Severson *et al*., 2018[39]. ChromHMM data was downloaded from
868 GSE73783 by Achinger-Kawecka *et al*., 2020[17].
869
870 **Data availability**
871 All sequencing data created in this study have been uploaded to the Gene Expression
872 Omnibus (GEO; https://www.ncbi.nlm.nih.gov/geo/) and are available under primary
873 accession code GSE171074. Biological material used in this study can be obtained
874 from the authors upon request.
875
876 **Code availability**
877 Python script language (v.2.7.8 and v.3.9.1) and R (v.3.6.3 and v.4.0.3) were used to
878 develop the bioinformatics methods and algorithms in this work. All code for Hi-C
879 and PCHi-C analyses is available within the GitHub repository
880 https://github.com/JoannaAch/PDX_Decitabine_3DEpigenome.
881
882 **Acknowledgments**

We thank members of the Clark Laboratory for helpful discussions and careful reading of the manuscript. We thank Arima Genomics Inc. for advice with performing Hi-C and Promoter Capture Hi-C in snap-frozen tumour tissues. S.J.C. is a National Health and Medical Research Council (NHMRC) Senior Principal Research Fellow #1063559. J.A-K. is a National Breast Cancer Foundation (NBCF) Mavis Robertson Fellow #IIRS-21-047. E.L. is a NBCF Endowed Chair. T.E.H. is an NBCF Fellow #IIRS-19-009. Q.D. is a NHMRC Investigator Grant recipient #1177792. This research was supported by the NHMRC Project Grant #1128916 (to S.J.C), Movember & National Breast Cancer Foundation Collaboration Initiative grant (MNBCF-17-012 to T.E.H., E.L., S.J.C.) and the Cancer Council NSW grants RG16-09 (to S.J.C) and RG20-04 (to J.A-K.). Research funding (to S.J.C.) was provided by Van Andel Institute through the Van Andel Institute – Stand Up To Cancer Epigenetics Dream Team. Stand Up To Cancer is a division of the Entertainment Industry Foundation, administered by AACR. The contents of the published material are solely the responsibility of the administering institution and individual authors and do not reflect the views of the NHMRC.

Author Contributions

Conception (S.J.C., C.S., J.A-K) and Experimental Design: J.A-K., K-M.C., N.P., T.E.H., E.L., C.S. and S.J.C. Methodology and Data Acquisition: J.A-K., K-M.C., N.P., E.C., A.Y., A.W., G.L.L., A.S., E.W. Data Analysis: J.A-K., E.C., H.H.M., S.C. and Q.D. Data Interpretation: J.A-K., K-M.C., N.P., E.C., Q.D., T.E.H., E.L., C.S. and S.J.C. Funding Acquisition: J.A-K., T.E.H., E.L. and S.J.C. Manuscript Writing: J.A-K. and S.J.C. with input from all authors.

Ethics declarations

A.S. is an employee of Arima Genomics, Inc. Other authors declare no competing interests.

References

1. Farcas, A.M., Nagarajan, S., Cosulich, S. & Carroll, J.S. Genome-Wide Estrogen Receptor Activity in Breast Cancer. *Endocrinology* **162**(2021).

916 2. Musgrove, E.A. & Sutherland, R.L. Biological determinants of endocrine
917 resistance in breast cancer. *Nat Rev Cancer* **9**, 631-43 (2009).

918 3. Ali, S. & Coombes, R.C. Endocrine-responsive breast cancer and strategies for
919 combating resistance. *Nat Rev Cancer* **2**, 101-12 (2002).

920 4. Ross-Innes, C.S. *et al.* Differential oestrogen receptor binding is associated
921 with clinical outcome in breast cancer. *Nature* **481**, 389-93 (2012).

922 5. Carroll, J.S. *et al.* Genome-wide analysis of estrogen receptor binding sites.
923 *Nat Genet* **38**, 1289-97 (2006).

924 6. Welboren, W.J. *et al.* ChIP-Seq of ERalpha and RNA polymerase II defines
925 genes differentially responding to ligands. *EMBO J* **28**, 1418-28 (2009).

926 7. Li, W. *et al.* Functional roles of enhancer RNAs for oestrogen-dependent
927 transcriptional activation. *Nature* **498**, 516-20 (2013).

928 8. Fullwood, M.J. *et al.* An oestrogen-receptor-alpha-bound human chromatin
929 interactome. *Nature* **462**, 58-64 (2009).

930 9. Lupien, M. *et al.* Growth factor stimulation induces a distinct ER(alpha)
931 cistrome underlying breast cancer endocrine resistance. *Genes Dev* **24**, 2219-
932 27 (2010).

933 10. Stone, A. *et al.* DNA methylation of oestrogen-regulated enhancers defines
934 endocrine sensitivity in breast cancer. *Nat Commun* **6**, 7758 (2015).

935 11. Achinger-Kawecka, J. & Clark, S.J. Disruption of the 3D cancer genome
936 blueprint. *Epigenomics* **9**, 47-55 (2017).

937 12. Taberlay, P.C. *et al.* Three-dimensional disorganization of the cancer genome
938 occurs coincident with long-range genetic and epigenetic alterations. *Genome*
939 *Res* **26**, 719-31 (2016).

940 13. Rhie, S.K. *et al.* A high-resolution 3D epigenomic map reveals insights into
941 the creation of the prostate cancer transcriptome. *Nat Commun* **10**, 4154
942 (2019).

943 14. Barutcu, A.R. *et al.* RUNX1 contributes to higher-order chromatin
944 organization and gene regulation in breast cancer cells. *Biochim Biophys Acta*
945 **1859**, 1389-1397 (2016).

946 15. Barutcu, A.R. *et al.* SMARCA4 regulates gene expression and higher-order
947 chromatin structure in proliferating mammary epithelial cells. *Genome Res* **26**,
948 1188-201 (2016).

949 16. Barutcu, A.R. *et al.* Chromatin interaction analysis reveals changes in small
950 chromosome and telomere clustering between epithelial and breast cancer
951 cells. *Genome Biol* **16**, 214 (2015).

952 17. Achinger-Kawecka, J. *et al.* Epigenetic reprogramming at estrogen-receptor
953 binding sites alters 3D chromatin landscape in endocrine-resistant breast
954 cancer. *Nat Commun* **11**, 320 (2020).

955 18. Zhou, Y. *et al.* Temporal dynamic reorganization of 3D chromatin architecture
956 in hormone-induced breast cancer and endocrine resistance. *Nat Commun* **10**,
957 1522 (2019).

958 19. Flavahan, W.A. *et al.* Insulator dysfunction and oncogene activation in IDH
959 mutant gliomas. *Nature* **529**, 110-4 (2016).

960 20. Kloetgen, A. *et al.* Three-dimensional chromatin landscapes in T cell acute
961 lymphoblastic leukemia. *Nat Genet* **52**, 388-400 (2020).

962 21. Vilarrasa-Blasi, R. *et al.* Dynamics of genome architecture and chromatin
963 function during human B cell differentiation and neoplastic transformation.
964 *Nat Commun* **12**, 651 (2021).

965 22. Corces, M.R. & Corces, V.G. The three-dimensional cancer genome. *Curr*
966 *Opin Genet Dev* **36**, 1-7 (2016).

967 23. Yang, Y. *et al.* The 3D Genomic Landscape of Differential Response to
968 EGFR/HER2 Inhibition in Endocrine-Resistant Breast Cancer Cells. *Biochim*
969 *Biophys Acta Gene Regul Mech*, 194631 (2020).

970 24. Bates, S.E. Epigenetic Therapies for Cancer. *N Engl J Med* **383**, 650-663
971 (2020).

972 25. Pandiyan, K. *et al.* Functional DNA demethylation is accompanied by
973 chromatin accessibility. *Nucleic Acids Res* **41**, 3973-85 (2013).

974 26. Yang, X. *et al.* Gene body methylation can alter gene expression and is a
975 therapeutic target in cancer. *Cancer Cell* **26**, 577-90 (2014).

976 27. Mehdipour, P. *et al.* Epigenetic therapy induces transcription of inverted
977 SINEs and ADAR1 dependency. *Nature* **588**, 169-+ (2020).

978 28. Roulois, D. *et al.* DNA-Demethylating Agents Target Colorectal Cancer Cells
979 by Inducing Viral Mimicry by Endogenous Transcripts. *Cell* **162**, 961-973
980 (2015).

981 29. Loo Yau, H. *et al.* DNA hypomethylating agents increase activation and
982 cytolytic activity of CD8(+) T cells. *Mol Cell* (2021).

983 30. Cazet, A.S. *et al.* Targeting stromal remodeling and cancer stem cell plasticity
984 overcomes chemoresistance in triple negative breast cancer. *Nat Commun* **9**,
985 2897 (2018).

986 31. Chia, K. *et al.* Non-canonical AR activity facilitates endocrine resistance in
987 breast cancer. *Endocr Relat Cancer* **26**, 251-264 (2019).

988 32. Portman, N. *et al.* MDM2 inhibition in combination with endocrine therapy
989 and CDK4/6 inhibition for the treatment of ER-positive breast cancer. *Breast*
990 *Cancer Research* **22**(2020).

991 33. Hickey, T.E. *et al.* The androgen receptor is a tumor suppressor in estrogen
992 receptor-positive breast cancer. *Nat Med* **27**, 310-320 (2021).

993 34. DeRose, Y.S. *et al.* Tumor grafts derived from women with breast cancer
994 authentically reflect tumor pathology, growth, metastasis and disease
995 outcomes. *Nat Med* **17**, 1514-20 (2011).

996 35. Zheng, Y. *et al.* Prediction of genome-wide DNA methylation in repetitive
997 elements. *Nucleic Acids Res* **45**, 8697-8711 (2017).

998 36. Subramanian, A. *et al.* Gene set enrichment analysis: a knowledge-based
999 approach for interpreting genome-wide expression profiles. *Proc Natl Acad*
1000 *Sci U S A* **102**, 15545-50 (2005).

1001 37. Hurtado, A., Holmes, K.A., Ross-Innes, C.S., Schmidt, D. & Carroll, J.S.
1002 FOXA1 is a key determinant of estrogen receptor function and endocrine
1003 response. *Nat Genet* **43**, 27-33 (2011).

1004 38. Carroll, J.S. *et al.* Chromosome-wide mapping of estrogen receptor binding
1005 reveals long-range regulation requiring the forkhead protein FoxA1. *Cell* **122**,
1006 33-43 (2005).

1007 39. Severson, T.M. *et al.* Characterizing steroid hormone receptor chromatin
1008 binding landscapes in male and female breast cancer. *Nat Commun* **9**, 482
1009 (2018).

1010 40. Lieberman-Aiden, E. *et al.* Comprehensive mapping of long-range interactions
1011 reveals folding principles of the human genome. *Science* **326**, 289-93 (2009).

1012 41. Cairns, J. *et al.* CHiCAGO: robust detection of DNA looping interactions in
1013 Capture Hi-C data. *Genome Biol* **17**, 127 (2016).

1014 42. Cairns, J., Orchard, W.R., Malysheva, V. & Spivakov, M. Chicdiff: a
1015 computational pipeline for detecting differential chromosomal interactions in
1016 Capture Hi-C data. *Bioinformatics* **35**, 4764-4766 (2019).

1017 43. Zuin, J. *et al.* Nonlinear control of transcription through enhancer-promoter
1018 interactions. *bioRxiv* (2021).

1019 44. Zhu, I., Song, W., Ovcharenko, I. & Landsman, D. A model of active
1020 transcription hubs that unifies the roles of active promoters and enhancers.
1021 *Nucleic Acids Res* (2021).

1022 45. Achinger-Kawecka, J., Chia, K-M., Portman, N., Campbell, E., Du, Q.,
1023 Laven-Law, G., Clifton, S., Milioli, H.H., Schmitt, A., Wong, E., Hickey, T.,
1024 Lim, E., Stirzaker, C., Clark, S.J. Epigenetic therapy suppresses tumour
1025 growth by rewiring ER-mediated long-range chromatin interactions in ER+
1026 endocrine-resistant breast cancer. *bioRxiv* (2021).

1027 46. Linnekamp, J.F., Butter, R., Spijker, R., Medema, J.P. & van Laarhoven,
1028 H.W.M. Clinical and biological effects of demethylating agents on solid
1029 tumours - A systematic review. *Cancer Treat Rev* **54**, 10-23 (2017).

1030 47. Oronsky, B., Oronsky, N., Knox, S., Fanger, G. & Scicinski, J.
1031 Episensitization: therapeutic tumor resensitization by epigenetic agents: a
1032 review and reassessment. *Anticancer Agents Med Chem* **14**, 1121-7 (2014).

1033 48. Garcia-Martinez, L., Zhang, Y., Nakata, Y., Chan, H.L. & Morey, L.
1034 Epigenetic mechanisms in breast cancer therapy and resistance. *Nat Commun*
1035 **12**, 1786 (2021).

1036 49. Tsai, H.C. *et al.* Transient Low Doses of DNA-Demethylating Agents Exert
1037 Durable Antitumor Effects on Hematological and Epithelial Tumor Cells.
1038 *Cancer Cell* **21**, 430-446 (2012).

1039 50. Lu, Z. *et al.* Epigenetic therapy inhibits metastases by disrupting premetastatic
1040 niches. *Nature* **579**, 284-290 (2020).

1041 51. Yu, J. *et al.* DNA methyltransferase expression in triple-negative breast cancer
1042 predicts sensitivity to decitabine. *J Clin Invest* **128**, 2376-2388 (2018).

1043 52. Dahn, M.L. *et al.* Decitabine Response in Breast Cancer Requires Efficient
1044 Drug Processing and Is Not Limited by Multidrug Resistance. *Mol Cancer*
1045 *Ther* **19**, 1110-1122 (2020).

1046 53. de Cubas, A.A. *et al.* DNA hypomethylation promotes transposable element
1047 expression and activation of immune signaling in renal cell cancer. *JCI Insight*
1048 **5**(2020).

1049 54. Johnstone, S.E. *et al.* Large-Scale Topological Changes Restrain Malignant
1050 Progression in Colorectal Cancer. *Cell* **182**, 1474-1489 e23 (2020).

1051 55. Lee, D.S. *et al.* Simultaneous profiling of 3D genome structure and DNA
1052 methylation in single human cells. *Nat Methods* **16**, 999-1006 (2019).

1053 56. Bell, A.C. & Felsenfeld, G. Methylation of a CTCF-dependent boundary
1054 controls imprinted expression of the Igf2 gene. *Nature* **405**, 482-5 (2000).

1055 57. Hark, A.T. *et al.* CTCF mediates methylation-sensitive enhancer-blocking
1056 activity at the H19/Igf2 locus. *Nature* **405**, 486-9 (2000).

1057 58. Maurano, M.T. *et al.* Role of DNA Methylation in Modulating Transcription
1058 Factor Occupancy. *Cell Rep* **12**, 1184-95 (2015).

1059 59. Ahmed, M. *et al.* CRISPRi screens reveal a DNA methylation-mediated 3D
1060 genome dependent causal mechanism in prostate cancer. *Nat Commun* **12**,
1061 1781 (2021).

1062 60. Du, Q. *et al.* DNA methylation is required to maintain DNA replication timing
1063 precision and 3D genome integrity. *bioRxiv* (2020).

1064 61. McLaughlin, K. *et al.* DNA Methylation Directs Polycomb-Dependent 3D
1065 Genome Re-organization in Naive Pluripotency. *Cell Rep* **29**, 1974-1985 e6
1066 (2019).

1067 62. Broome, R. *et al.* TET2 is a component of the estrogen receptor complex and
1068 controls 5mC to 5hmC conversion at estrogen receptor cis-regulatory regions.
1069 *Cell Rep* **34**, 108776 (2021).

1070 63. Bi, M. *et al.* Enhancer reprogramming driven by high-order assemblies of
1071 transcription factors promotes phenotypic plasticity and breast cancer
1072 endocrine resistance. *Nat Cell Biol* **22**, 701-715 (2020).

1073 64. Nagarajan, S. *et al.* ARID1A influences HDAC1/BRD4 activity, intrinsic
1074 proliferative capacity and breast cancer treatment response. *Nat Genet* **52**,
1075 187-197 (2020).

1076 65. Schmitt, A.D. *et al.* A Compendium of Chromatin Contact Maps Reveals
1077 Spatially Active Regions in the Human Genome. *Cell Rep* **17**, 2042-2059
1078 (2016).

1079 66. Oudelaar, A.M. *et al.* A revised model for promoter competition based on
1080 multi-way chromatin interactions at the alpha-globin locus. *Nat Commun* **10**,
1081 5412 (2019).

1082 67. Thomas, H.F. *et al.* Temporal dissection of an enhancer cluster reveals distinct
1083 temporal and functional contributions of individual elements. *Mol Cell* (2021).

1084 68. DeRose, Y.S. *et al.* Tumor grafts derived from women with breast cancer
1085 authentically reflect tumor pathology, growth, metastasis and disease
1086 outcomes. *Nature Medicine* **17**, 1514-U227 (2011).

1087 69. Schoenfelder, S. *et al.* The pluripotent regulatory circuitry connecting
1088 promoters to their long-range interacting elements. *Genome Res* **25**, 582-97
1089 (2015).

1090 70. Schoenfelder, S., Javierre, B.M., Furlan-Magaril, M., Wingett, S.W. & Fraser,
1091 P. Promoter Capture Hi-C: High-resolution, Genome-wide Profiling of
1092 Promoter Interactions. *Jove-Journal of Visualized Experiments* (2018).

1093 71. Schoenfelder, S. *et al.* Polycomb repressive complex PRC1 spatially
1094 constrains the mouse embryonic stem cell genome. *Nat Genet* **47**, 1179-1186
1095 (2015).

1096 72. Aryee, M.J. *et al.* Minfi: a flexible and comprehensive Bioconductor package
1097 for the analysis of Infinium DNA methylation microarrays. *Bioinformatics* **30**,
1098 1363-9 (2014).

1099 73. Pidsley, R. *et al.* Critical evaluation of the Illumina MethylationEPIC
1100 BeadChip microarray for whole-genome DNA methylation profiling. *Genome*
1101 *Biol* **17**, 208 (2016).

1102 74. Zhou, W.D., Laird, P.W. & Shen, H. Comprehensive characterization,
1103 annotation and innovative use of Infinium DNA methylation BeadChip probes.
1104 *Nucleic Acids Research* **45**(2017).

1105 75. Ritchie, M.E. *et al.* limma powers differential expression analyses for RNA-
1106 sequencing and microarray studies. *Nucleic Acids Res* **43**, e47 (2015).

1107 76. Peters, T.J. *et al.* De novo identification of differentially methylated regions in
1108 the human genome. *Epigenetics Chromatin* **8**, 6 (2015).

1109 77. Wingett, S.W. & Andrews, S. FastQ Screen: A tool for multi-genome
1110 mapping and quality control. *F1000Res* **7**, 1338 (2018).

1111 78. Conway, T. *et al.* Xenome--a tool for classifying reads from xenograft
1112 samples. *Bioinformatics* **28**, i172-8 (2012).

1113 79. Dozmorov, M.G. *et al.* Chromatin conformation capture (Hi-C) sequencing of
1114 patient-derived xenografts: analysis guidelines. *Gigascience* **10**(2021).

1115 80. Servant, N. *et al.* HiC-Pro: an optimized and flexible pipeline for Hi-C data
1116 processing. *Genome Biology* **16**(2015).

1117 81. Imakaev, M. *et al.* Iterative correction of Hi-C data reveals hallmarks of
1118 chromosome organization. *Nat Methods* **9**, 999-1003 (2012).

1119 82. Wu, P. *et al.* 3D genome of multiple myeloma reveals spatial genome
1120 disorganization associated with copy number variations. *Nat Commun* **8**, 1937
1121 (2017).

1122 83. Durand, N.C. *et al.* Juicer Provides a One-Click System for Analyzing Loop-
1123 Resolution Hi-C Experiments. *Cell Syst* **3**, 95-8 (2016).

1124 84. Durand, N.C. *et al.* Juicebox Provides a Visualization System for Hi-C
1125 Contact Maps with Unlimited Zoom. *Cell Syst* **3**, 99-101 (2016).

1126 85. Zhou, X. *et al.* Exploring long-range genome interactions using the WashU
1127 Epigenome Browser. *Nat Methods* **10**, 375-6 (2013).

1128 86. Kruse, K., Hug, C.B., Hernandez-Rodriguez, B. & Vaquerizas, J.M. TADtool:
1129 visual parameter identification for TAD-calling algorithms. *Bioinformatics* **32**,
1130 3190-3192 (2016).

1131 87. van der Weide, R.H. *et al.* Hi-C Analyses with GENOVA: a case study with
1132 cohesin variants. *bioRxiv* (2021).

1133 88. Wingett, S. *et al.* HiCUP: pipeline for mapping and processing Hi-C data.
1134 *F1000Res* **4**, 1310 (2015).

1135 89. Blighe K, S.R., M Lewis. EnhancedVolcano: Publication-ready volcano plots
1136 with enhanced colouring and labeling. (2018).

1137 90. Dobin, A. *et al.* STAR: ultrafast universal RNA-seq aligner. *Bioinformatics* **29**,
1138 15-21 (2013).

1139 91. Robinson, M.D. & Oshlack, A. A scaling normalization method for
1140 differential expression analysis of RNA-seq data. *Genome Biol* **11**, R25 (2010).

1141 92. Robinson, M.D., McCarthy, D.J. & Smyth, G.K. edgeR: a Bioconductor
1142 package for differential expression analysis of digital gene expression data.
1143 *Bioinformatics* **26**, 139-40 (2010).

1144 93. Jin, Y., Tam, O.H., Paniagua, E. & Hammell, M. TEtranscripts: a package for
1145 including transposable elements in differential expression analysis of RNA-
1146 seq datasets. *Bioinformatics* **31**, 3593-3599 (2015).

1147 94. Love, M.I., Huber, W. & Anders, S. Moderated estimation of fold change and
1148 dispersion for RNA-seq data with DESeq2. *Genome Biology* **15**(2014).

1149 95. Langmead, B., Trapnell, C., Pop, M. & Salzberg, S.L. Ultrafast and memory-
1150 efficient alignment of short DNA sequences to the human genome. *Genome*
1151 *Biol* **10**, R25 (2009).

1152 96. Zhang, Y. *et al.* Model-based analysis of ChIP-Seq (MACS). *Genome Biol* **9**,
1153 R137 (2008).

1154 97. Feng, J.X., Liu, T., Qin, B., Zhang, Y. & Liu, X.S. Identifying ChIP-seq
1155 enrichment using MACS. *Nature Protocols* **7**, 1728-1740 (2012).

1156 98. Heger, A., Webber, C., Goodson, M., Ponting, C.P. & Lunter, G. GAT: a
1157 simulation framework for testing the association of genomic intervals.
1158 *Bioinformatics* **29**, 2046-8 (2013).

1159 99. Yu, G., Wang, L.G. & He, Q.Y. ChIPseeker: an R/Bioconductor package for
1160 ChIP peak annotation, comparison and visualization. *Bioinformatics* **31**, 2382-
1161 3 (2015).

1162 100. Ramirez, F. *et al.* deepTools2: a next generation web server for deep-
1163 sequencing data analysis. *Nucleic Acids Res* **44**, W160-5 (2016).

1164 101. Heinz, S. *et al.* Simple Combinations of Lineage-Determining Transcription
1165 Factors Prime cis-Regulatory Elements Required for Macrophage and B Cell
1166 Identities. *Molecular Cell* **38**, 576-589 (2010).

1167 102. Curtis, C. *et al.* The genomic and transcriptomic architecture of 2,000 breast
1168 tumours reveals novel subgroups. *Nature* **486**, 346-52 (2012).

1169 103. Pereira, B. *et al.* The somatic mutation profiles of 2,433 breast cancers refines
1170 their genomic and transcriptomic landscapes. *Nat Commun* **7**, 11479 (2016).

1171 104. Berger, A.C. *et al.* A Comprehensive Pan-Cancer Molecular Study of
1172 Gynecologic and Breast Cancers. *Cancer Cell* **33**, 690-705 e9 (2018).

1173 105. Ciriello, G. *et al.* Comprehensive Molecular Portraits of Invasive Lobular
1174 Breast Cancer. *Cell* **163**, 506-19 (2015).

1175 106. Cerami, E. *et al.* The cBio cancer genomics portal: an open platform for
1176 exploring multidimensional cancer genomics data. *Cancer Discov* **2**, 401-4
1177 (2012).

1178

Fig. 1

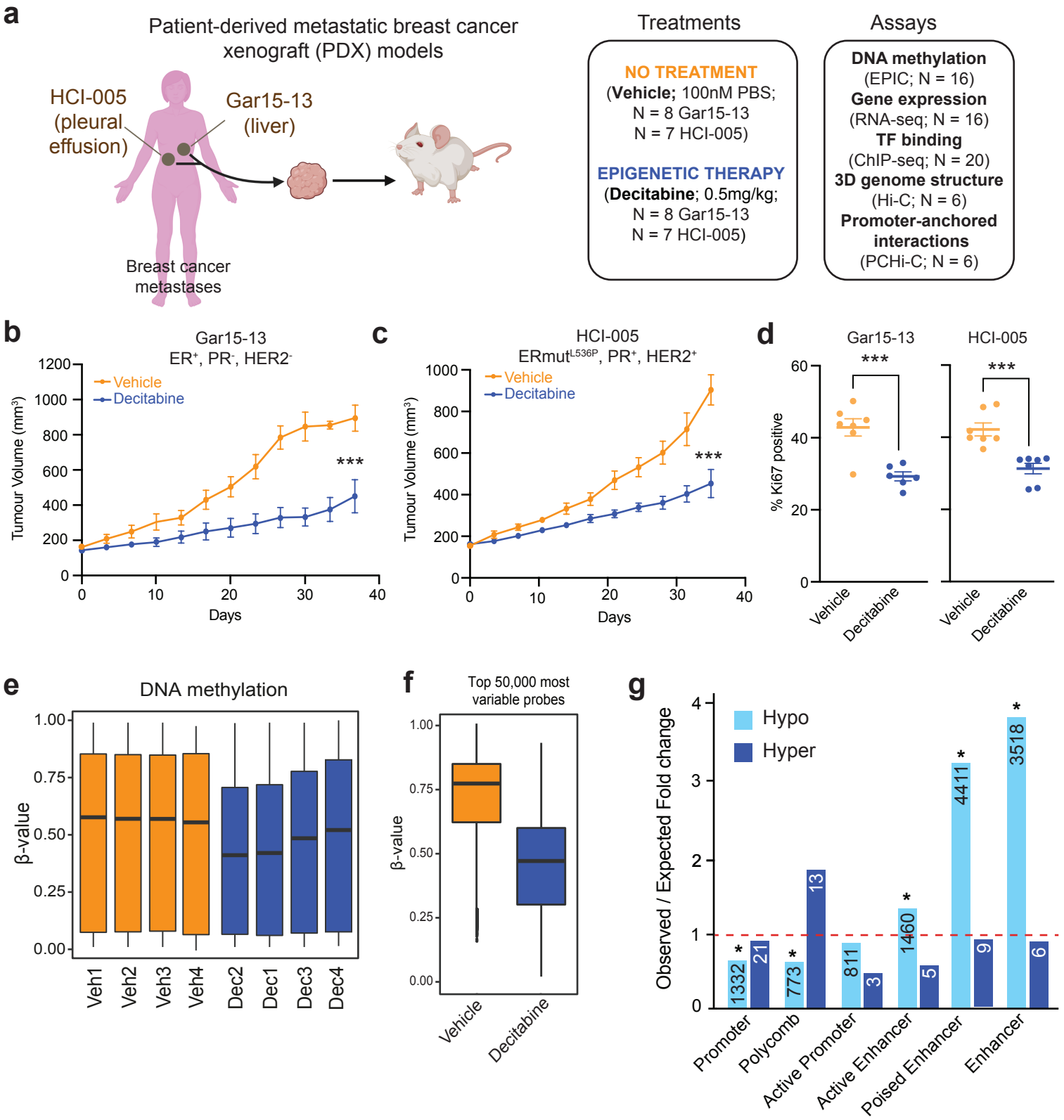
a
Patient-derived metastatic breast cancer xenograft (PDX) models
HCI-005 (pleural effusion)
Gar15-13 (liver)
Breast cancer metastases
Treatments
NO TREATMENT
(Vehicle; 100nM PBS;
N = 8 Gar15-13
N = 7 HCI-005)
EPIGENETIC THERAPY
(Decitabine; 0.5mg/kg;
N = 8 Gar15-13
N = 7 HCI-005)
Assays
DNA methylation
(EPIC; N = 16)
Gene expression
(RNA-seq; N = 16)
TF binding
(ChIP-seq; N = 20)
3D genome structure
(Hi-C; N = 6)
Promoter-anchored interactions
(PCHi-C; N = 6)
b
Gar15-13
ER+, PR-, HER2-
Vehicle
Decitabine
Tumour Volume (mm3)
Days
***
c
HCI-005
ERmutL536P, PR+, HER2+
Vehicle
Decitabine
Tumour Volume (mm3)
Days
***
d
Gar15-13
HCI-005
% Ki67 positive
***
Vehicle
Decitabine
e
DNA methylation
β-value
Veh1
Veh2
Veh3
Veh4
Dec2
Dec1
Dec3
Dec4
f
Top 50,000 most variable probes
β-value
Vehicle
Decitabine
g
Hypo
Hyper
Observed / Expected Fold change
Promoter
Polycomb
Active Promoter
Active Enhancer
Poised Enhancer
Enhancer
1332
21
773
13
811
3
1460
5
4411
9
3518
6

Fig. 1 Decitabine supresses tumour growth and proliferation markers in PDX models of endocrine-resistant ER+ breast cancer.

(a) Schematic of models and treatments used in the study and summary of genome-wide assays applied to PDX tumours at end-point.

(b) Growth of treatment naïve (Vehicle) (100nM PBS, n = 7) and Decitabine-treated (0.5mg/kg, n = 7) Gar15-13 PDX tumours for 35 days or until ethical endpoint. All data are mean ± SEM. *** P value < 0.001.

(c) Growth of treatment naïve (Vehicle) (100nM PBS, n = 8), and Decitabine-treated (0.5mg/kg, n = 7) HCI-005 PDX tumours for 35 days or until ethical endpoint. All data are mean ± SEM. *** P value < 0.001.

(d) Quantification of the proliferation marker Ki-67 at endpoint in Gar15-13 and HCI-005 tumours. Ki-67 proportions from all replicates per treatment were compared by two-tailed T test. *P value < 0.001.

(e) Boxplots showing the distribution of DNA methylation profiles for Gar15-13 Vehicle and Decitabine-treated tumours for all EPIC probes across the genome. Black line indicates mean ± SD.

(f) Boxplots showing DNA methylation distribution for the 50,000 most variably methylated probes in Vehicle compared to Decitabine for Gar15-13 tumours. Black line indicates mean ± SD.

(g) Bar plot showing the association of differentially methylated probes in Gar15-13 Decitabine treatment compared to Vehicle across different regulatory regions of the genome as determined by TAMR ChromHMM annotation. Observed over expected fold change enrichment shown. * P value < 0.001. The numbers of hypo/hypermethylated probes located within each specific region are presented in the respective column.

Fig. 2

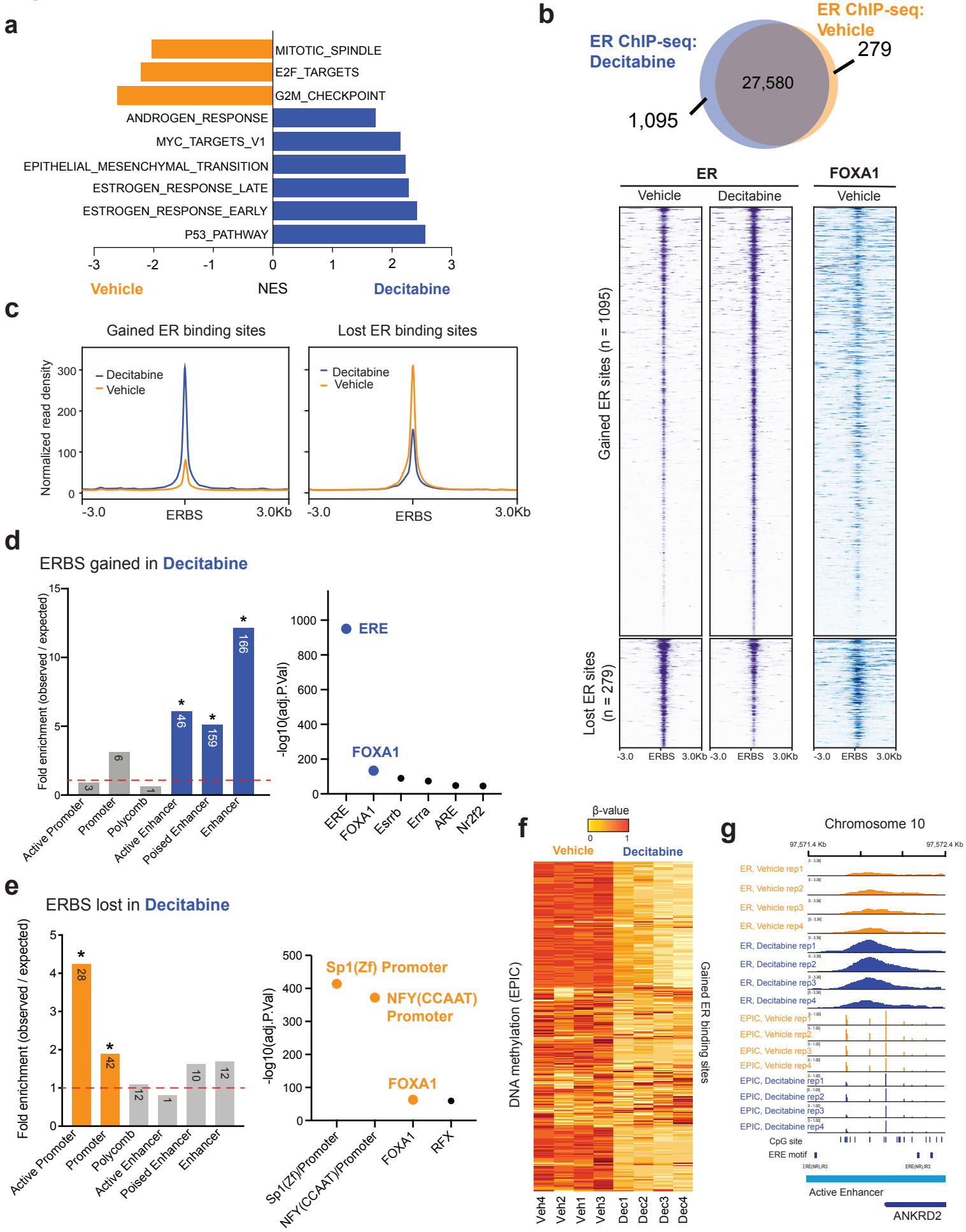
a
MITOTIC_SPINDLE
E2F_TARGETS
G2M_CHECKPOINT
ANDROGEN_RESPONSE
MYC_TARGETS_V1
EPITHELIAL_MESENCHYMAL_TRANSITION
ESTROGEN_RESPONSE_LATE
ESTROGEN_RESPONSE_EARLY
P53_PATHWAY
-3 -2 -1 0 1 2 3
Vehicle
NES
Decitabine
b
ER ChIP-seq: Vehicle
ER ChIP-seq: Decitabine
279
27,580
1,095
ER
FOXA1
Vehicle
Decitabine
Vehicle
Gained ER sites (n = 1095)
Lost ER sites (n = 279)
-3.0 ERBS 3.0Kb
c
Gained ER binding sites
Lost ER binding sites
Normalized read density
Decitabine
Vehicle
300
200
100
0
-3.0 ERBS 3.0Kb
d
ERBS gained in Decitabine
Fold enrichment (observed / expected)
15
10
5
0
3
6
1
46
159
166
Active Promoter
Promoter
Polycomb
Active Enhancer
Poised Enhancer
Enhancer
-log10(adj.P.Val)
1000
800
600
400
200
0
ERE
FOXA1
ERE
FOXA1
Esrrb
Erra
ARE
Nr2f2
e
ERBS lost in Decitabine
Fold enrichment (observed / expected)
5
4
3
2
1
0
28
42
12
1
10
12
Active Promoter
Promoter
Polycomb
Active Enhancer
Poised Enhancer
Enhancer
-log10(adj.P.Val)
500
400
300
200
100
0
Sp1(Zf) Promoter
NFY(CCAAT) Promoter
FOXA1
Sp1(Zf)/Promoter
NFY(CCAAT)/Promoter
FOXA1
RFX
f
β-value
0
1
Vehicle
Decitabine
DNA methylation (EPIC)
Gained ER binding sites
Veh4
Veh2
Veh1
Veh3
Dec1
Dec2
Dec3
Dec4
g
Chromosome 10
97,571.4 Kb
97,572.4 Kb
ER, Vehicle rep1
ER, Vehicle rep2
ER, Vehicle rep3
ER, Vehicle rep4
ER, Decitabine rep1
ER, Decitabine rep2
ER, Decitabine rep3
ER, Decitabine rep4
EPIC, Vehicle rep1
EPIC, Vehicle rep2
EPIC, Vehicle rep3
EPIC, Vehicle rep4
EPIC, Decitabine rep1
EPIC, Decitabine rep2
EPIC, Decitabine rep3
EPIC, Decitabine rep4
CpG site
ERE motif
Active Enhancer
ANKRD2

Fig. 2 Decitabine-induced DNA hypomethylation reprograms the ER cistrome.
(a) Normalized enrichment scores (NES) for signature gene sets representing differentially expressed genes in RNA-seq data from Gar15-13 PDX tumours treated with Decitabine compared to Vehicle (n = 4; FDR < 0.05)
(b) Overlap of consensus ER cistromes in Vehicle and Decitabine-treated Gar15-13 PDX tumours (n = 4 each). Heatmaps indicate ER ChIP-seq signal intensity at ER binding sites gained and lost in Decitabine compared to Vehicle-treated tumours and FOXA1 ChIP-seq signal intensity in Vehicle tumours.
(c) Average signal intensity of ER ChIP-seq binding (Gar15-13 Vehicle and Decitabine tumours) at gained and lost ER binding sites with Decitabine treatment.
(d) ChromHMM (TAMR) annotation (**P* value < 0.001) and motifs enriched at ER binding sites gained with Decitabine treatment compared to matched random regions generated from ERE binding motifs across the genome. Size of the overlap is presented in the respective column.
(e) ChromHMM (TAMR) annotation (**P* value < 0.001) and motifs enriched at ER binding sites lost with Decitabine treatment compared to matched random regions generated from ERE binding motifs across the genome. Size of the overlap is presented in the respective column.
(f) Heatmap showing DNA methylation levels (β-values) at gained ER binding sites in Decitabine-treated (n = 4) and Vehicle (n = 4) PDX tumours.
(g) Browser snapshot of ER ChIP-seq together with EPIC DNA methylation (Vehicle and Decitabine treatment, n = 4 each) showing gain of ER binding and loss of DNA methylation at an enhancer region of ER target gene *ANKRD2*.

Fig. 3

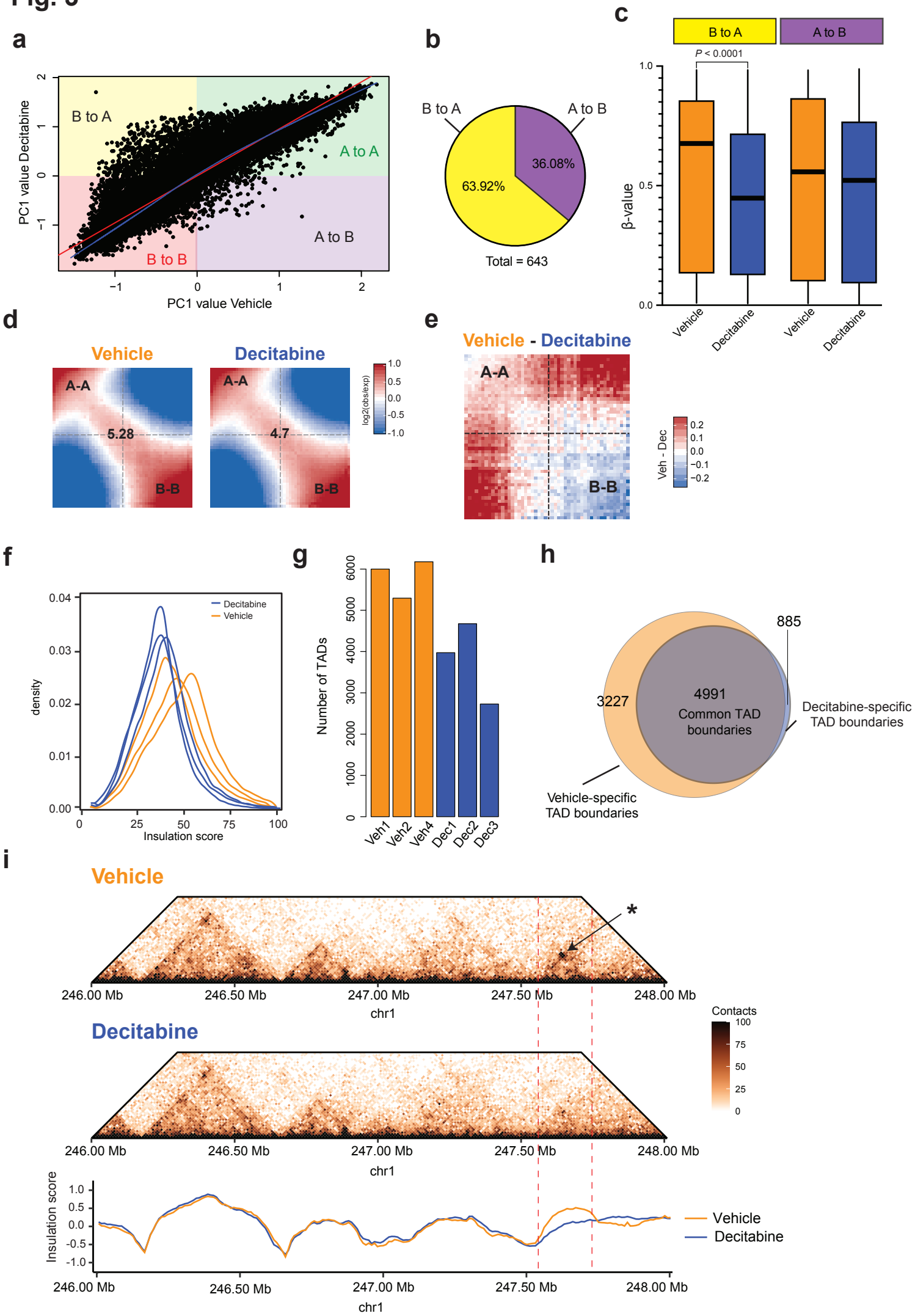
a
B to A
A to A
A to B
B to B
PC1 value Decitabine
PC1 value Vehicle
b
B to A
A to B
36.08%
63.92%
Total = 643
c
B to A
A to B
P < 0.0001
β-value
Vehicle
Decitabine
Vehicle
Decitabine
d
Vehicle
Decitabine
A-A
B-B
5.28
4.7
log2(obs/exp)
e
Vehicle - Decitabine
A-A
B-B
Veh - Dec
f
Decitabine
Vehicle
density
Insulation score
g
Number of TADs
Veh1
Veh2
Veh4
Dec1
Dec2
Dec3
h
885
3227
4991
Common TAD boundaries
Decitabine-specific TAD boundaries
Vehicle-specific TAD boundaries
i
Vehicle
Decitabine
246.00 Mb
246.50 Mb
247.00 Mb
247.50 Mb
248.00 Mb
chr1
Contacts
Insulation score
Vehicle
Decitabine

Fig. 3 Loss of DNA methylation results in de-compaction of chromatin.

(a) Scatterplot showing correlation between average eigenvalues per bin in Vehicle and Decitabine-treated Gar15-13 PDX tumours.

(b) Pie chart showing distribution of different types of switching compartments (A to B; B to A) in Decitabine-treated tumours as compared to Vehicle.

(c) Boxplot showing DNA methylation levels at compartment regions that switched their assignment from B to A and from A to B in Decitabine-treated (n = 4) and Vehicle (n = 4) PDX tumours. Black line indicates mean ± SD.

(d) Average contact enrichment (saddle plots) between pairs of 50Kb loci arranged by their PC1 eigenvector in Vehicle and Decitabine-treated tumours. Average data from n = 3 Hi-C replicates for Vehicle and Decitabine shown. The numbers at the centre of the heatmaps indicate compartment strength calculated as the log2 transformed ratio of (A–A + B–B)/ (A–B + B–A) using the mean values.

(e) Difference in Hi-C data between Vehicle and Decitabine treatments. Saddle plots were calculated using the averaged PC1 obtained from Vehicle (n = 3) and Decitabine-treated (n = 3) tumours.

(f) Density plot of insulation scores calculated in Vehicle and Decitabine-treated tumours.

(g) Number of TADs identified in Vehicle (n = 3) and Decitabine-treated (n = 3) PDX tumours.

(h) Venn diagram showing overlap between TAD boundaries identified in Vehicle and Decitabine-treated tumours.

(i) Snapshot of region on chromosome 1, showing Vehicle (top panel) and Decitabine-treated tumour Hi-C matrixes (bottom panel), demonstrating loss of a TAD in Decitabine-treated samples (indicated with an arrow), concomitant with decreased insulation at that region. Merged Hi-C data from replicates (n = 3 each) shown at 10Kb resolution.

Fig. 4

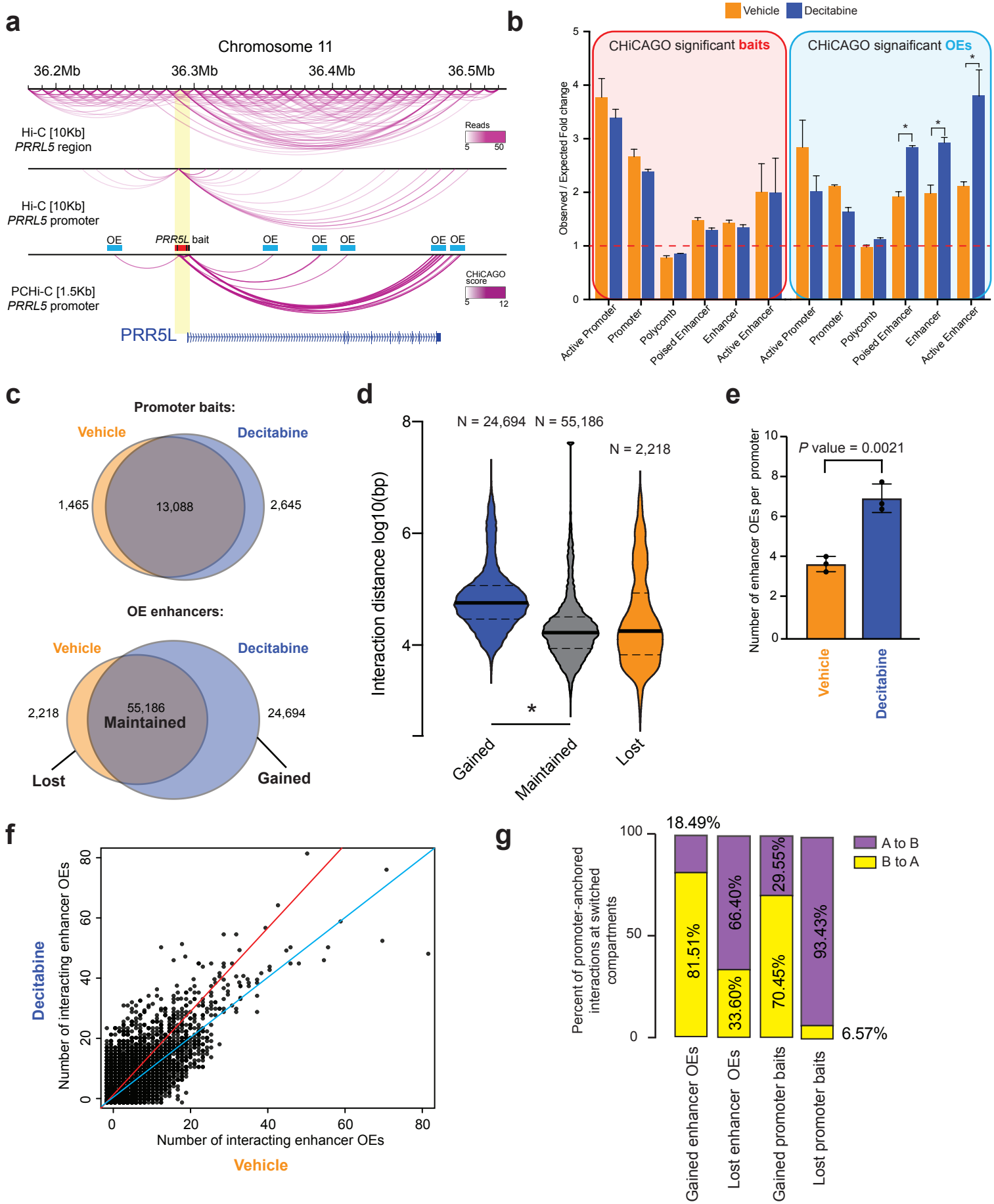
a
Chromosome 11
36.2Mb
36.3Mb
36.4Mb
36.5Mb
Hi-C [10Kb]
PRRL5 region
Reads
5
50
Hi-C [10Kb]
PRRL5 promoter
OE
PRR5L bait
OE
OE
OE
OE
OE
PCHi-C [1.5Kb]
PRRL5 promoter
CHiCAGO score
5
12
PRR5L
b
Vehicle
Decitabine
CHiCAGO significant baits
CHiCAGO signaificant OEs
Observed / Expected Fold change
Active Promoter
Promoter
Polycomb
Poised Enhancer
Enhancer
Active Enhancer
c
Promoter baits:
Vehicle
Decitabine
1,465
13,088
2,645
OE enhancers:
Vehicle
Decitabine
2,218
55,186
Maintained
24,694
Lost
Gained
d
N = 24,694
N = 55,186
N = 2,218
Interaction distance log10(bp)
Gained
Maintained
Lost
e
P value = 0.0021
Number of enhancer OEs per promoter
Vehicle
Decitabine
f
Decitabine
Number of interacting enhancer OEs
Number of interacting enhancer OEs
Vehicle
g
Percent of promoter-anchored interactions at switched compartments
18.49%
81.51%
66.40%
33.60%
29.55%
70.45%
93.43%
6.57%
A to B
B to A
Gained enhancer OEs
Lost enhancer OEs
Gained promoter baits
Lost promoter baits

Fig. 4 Loss of DNA methylation rewires long-range promoter-anchored enhancer interactions.

(a) Browser snapshot of interactions landscape at the *PRR5L* gene demonstrating increased coverage of promoter-anchored interactions in PCHi-C at 1.5Kb resolution compared to Hi-C at 10Kb resolution. Bait and other end (OE) regions marked for illustrative purposes.

(b) ChromHMM (TAMR) annotation of CHiCAGO significant interaction bait (promoter) and other end (OEs) regions (putative enhancers) in Decitabine-treated and Vehicle samples (* *P* value < 0.001)

(c) Overlap between promoter bait and other end (OE) enhancer regions for CHiCAGO significant interactions in Vehicle and Decitabine-treated tumours. Merged data across replicates shown.

(d) Violin plots showing the log10 genomic distance of promoter interactions whose enhancer OEs are gained, maintained or lost following Decitabine treatment. *P* value < 0.0001, Wilcoxon test. Merged data across replicates shown.

(e) Average number of enhancer OE interactions per promoter bait. Error bars indicate the interquartile range. *P* value Wilcoxon test.

(f) Scatterplot showing number of enhancer OE interactions per promoter bait for each CHiCAGO significant promoter-anchored interaction in Vehicle and Decitabine-treated tumours. Merged data across replicates shown.

(g) Percent of overlap of promoter baits and enhancer OEs that are either gained or lost in Decitabine with compartment that switch with Decitabine (A to B or B to A).

Fig. 5

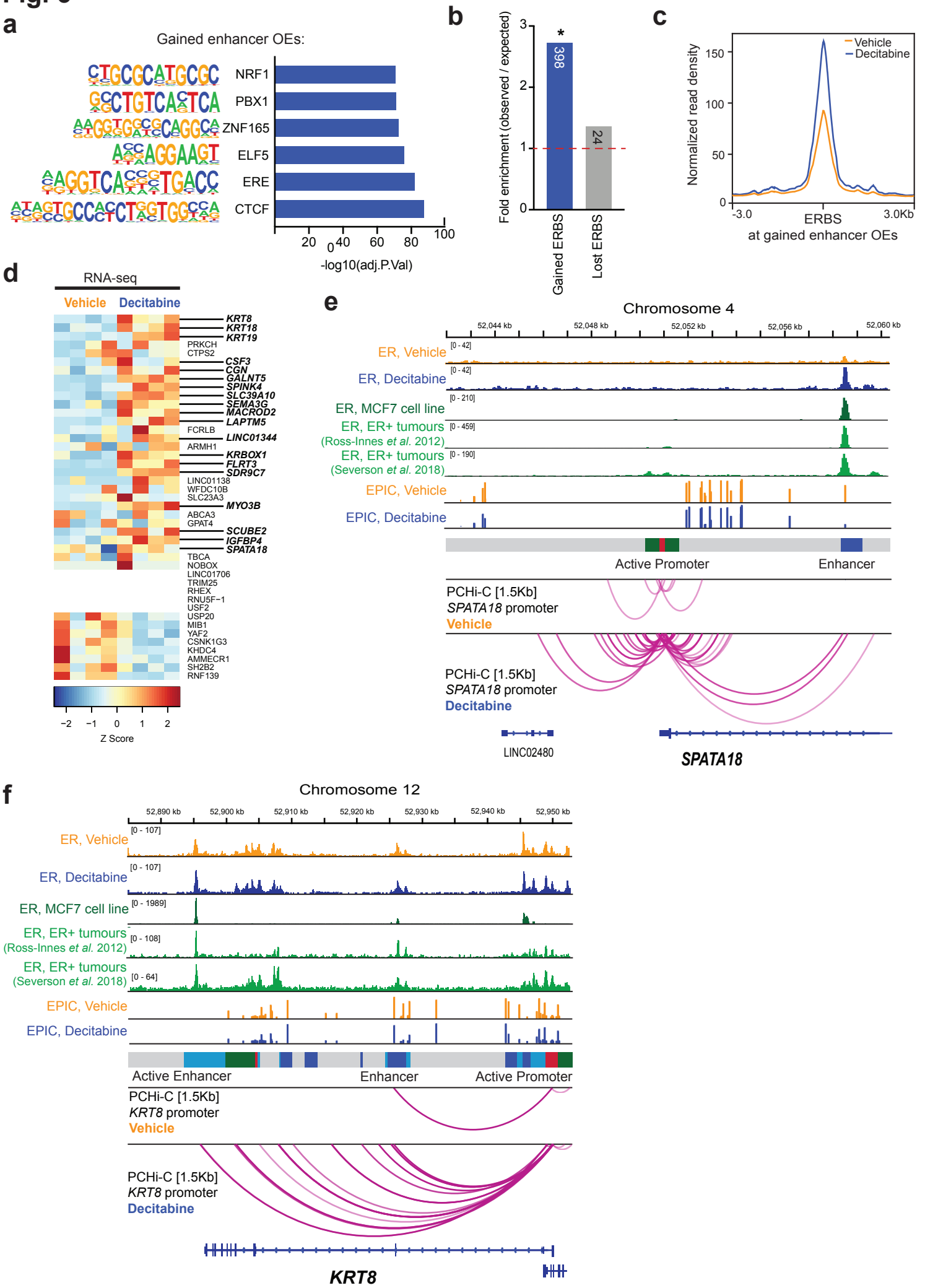
a
Gained enhancer OEs:
NRF1
PBX1
ZNF165
ELF5
ERE
CTCF
-log10(adj.P.Val)
b
Fold enrichment (observed / expected)
398
24
Gained ERBS
Lost ERBS
c
Vehicle
Decitabine
Normalized read density
ERBS
at gained enhancer OEs
-3.0
3.0Kb
d
RNA-seq
Vehicle
Decitabine
KRT8
KRT18
KRT19
PRKCH
CTPS2
CSF3
CGN
GALNT5
SPINK4
SLC39A10
SEMA3G
MACROD2
LAPTM5
FCRLB
LINC01344
ARMH1
KRBOX1
FLRT3
SDR9C7
LINC01138
WFDC10B
SLC23A3
MYO3B
ABCA3
GPAT4
SCUBE2
IGFBP4
SPATA18
TBCA
NOBOX
LINC01706
TRIM25
RHEX
RNU5F-1
USF2
USP20
MIB1
YAF2
CSNK1G3
KHDC4
AMMECR1
SH2B2
RNF139
Z Score
e
Chromosome 4
ER, Vehicle
ER, Decitabine
ER, MCF7 cell line
ER, ER+ tumours (Ross-Innes et al. 2012)
ER, ER+ tumours (Severson et al. 2018)
EPIC, Vehicle
EPIC, Decitabine
Active Promoter
Enhancer
PCHi-C [1.5Kb] SPATA18 promoter Vehicle
PCHi-C [1.5Kb] SPATA18 promoter Decitabine
LINC02480
SPATA18
f
Chromosome 12
ER, Vehicle
ER, Decitabine
ER, MCF7 cell line
ER, ER+ tumours (Ross-Innes et al. 2012)
ER, ER+ tumours (Severson et al. 2018)
EPIC, Vehicle
EPIC, Decitabine
Active Enhancer
Enhancer
Active Promoter
PCHi-C [1.5Kb] KRT8 promoter Vehicle
PCHi-C [1.5Kb] KRT8 promoter Decitabine
KRT8

Fig. 5 Rewired promoter-anchored interactions connect ER-bound enhancers to ER target genes.

(a) Transcription factor motifs significantly enriched at promoter-interacting enhancers (enhancer OEs) gained with Decitabine treatment. Only motifs with FDR < 0.05 are shown.

(b) Observed/expected fold change enrichment of gained enhancer OEs for ER binding gained and lost following Decitabine treatment. * *P* value < 0.0001.

(c) Average ER ChIP-seq signal intensity (Gar15-13 Vehicle and Decitabine-treated tumours) at ER binding sites located at DNA hypomethylation-induced enhancer OEs.

(d) Heatmap showing expression of genes connected to gained ER-mediated enhancer OEs in Vehicle and Decitabine-treated tumours. Genes in bold are significantly upregulated following Decitabine treatment and belong to a gene signature identified in our study.

(e) Browser snapshots showing the promoter-anchored interactions at the *SPATA18* gene, together with the average ER ChIP-seq signal, EPIC DNA methylation and ChromHMM track. Merged replicate data shown (n = 4 each). In Decitabine-treated tumours, the *SPATA18* promoter displays an increased number of interactions with an upstream enhancer region, which gains ER binding with Decitabine treatment, concomitant with loss of DNA methylation. This gained ER binding site is also present in ER ChIP-seq data representing primary ER+ breast tumours from Ross-Innes *et al.,* 2012 and Severson *et al.,* 2018. Expression of the *SPATA18* gene was significantly upregulated in Decitabine-treated tumours (shown in Data Fig. 5b).

(f) Browser snapshots showing promoter-anchored interactions at the *KRT8* ER target gene, together with ER ChIP-seq, EPIC DNA methylation and ChromHMM track. Merged replicate data shown (n = 4 each). In Decitabine-treated tumours, the *KRT8* promoter displays an increased number of interactions with multiple enhancers, one of which gains ER binding with Decitabine treatment. This gained ER binding site is also present in ER ChIP-seq data from primary ER+ breast tumours from Ross-Innes *et al.,* 2012 and Severson *et al.,* 2018. Expression of the *KRT8* gene was significantly upregulated in Decitabine-treated tumours (shown in Extended Data Fig. 5e).

Fig. 6

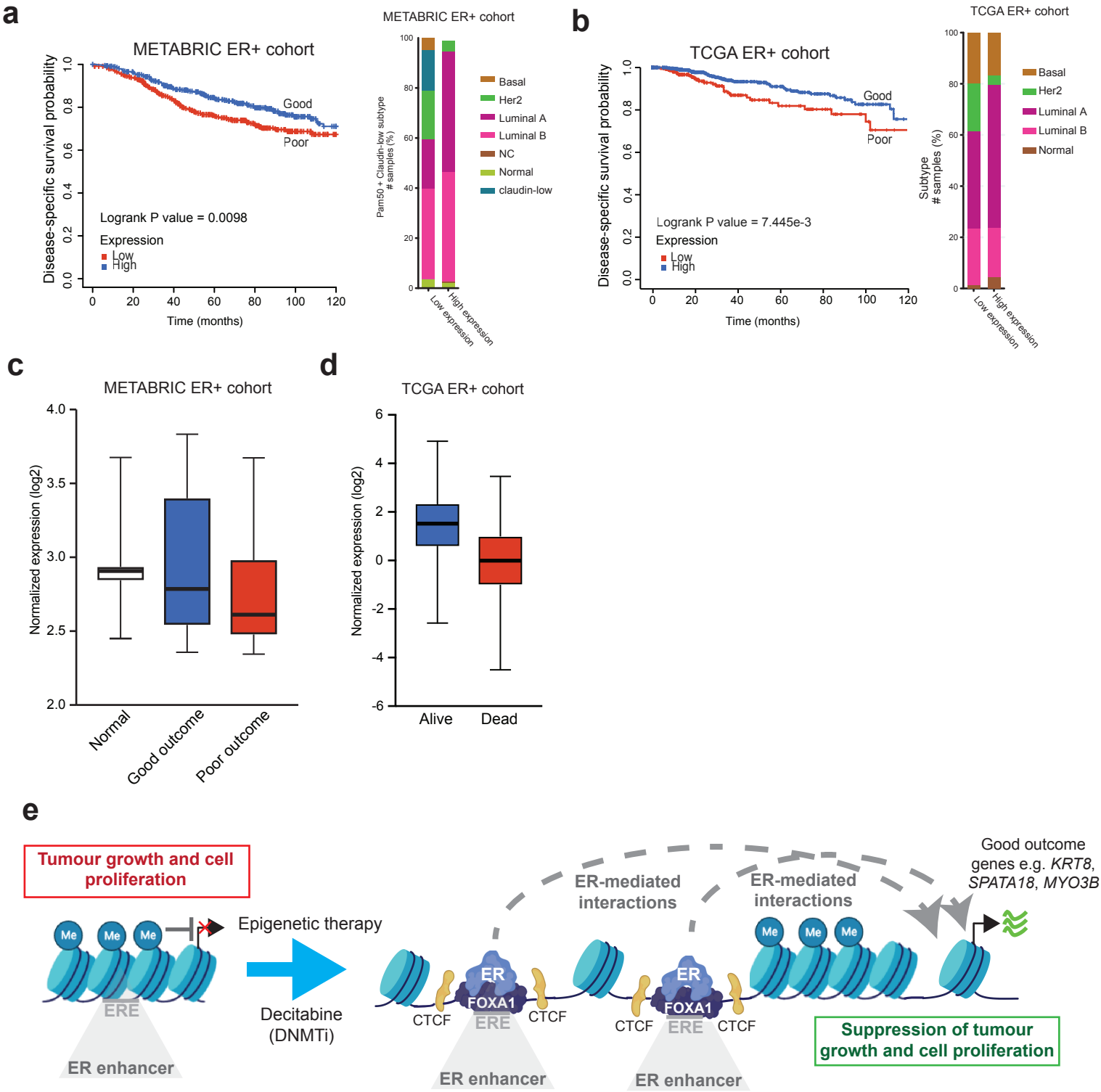
a
METABRIC ER+ cohort
Disease-specific survival probability
Good
Poor
Logrank P value = 0.0098
Expression
Low
High
Time (months)
METABRIC ER+ cohort
Pam50 + Claudin-low subtype # samples (%)
Basal
Her2
Luminal A
Luminal B
NC
Normal
claudin-low
Low expression
High expression
b
TCGA ER+ cohort
Disease-specific survival probability
Good
Poor
Logrank P value = 7.445e-3
Expression
Low
High
Time (months)
TCGA ER+ cohort
Subtype # samples (%)
Basal
Her2
Luminal A
Luminal B
Normal
Low expression
High expression
c
METABRIC ER+ cohort
Normalized expression (log2)
Normal
Good outcome
Poor outcome
d
TCGA ER+ cohort
Normalized expression (log2)
Alive
Dead
e
Tumour growth and cell proliferation
Me
ERE
ER enhancer
Epigenetic therapy
Decitabine (DNMTi)
ER-mediated interactions
ER-mediated interactions
ER
FOXA1
CTCF
ERE
CTCF
ER enhancer
Good outcome genes e.g. KRT8, SPATA18, MYO3B
Suppression of tumour growth and cell proliferation

Fig. 6 ER target gene signature is prognostic in ER+ breast cancer.

(a) Kaplan–Meier survival plot showing ability of the gene signature identified in our study (n = 17 genes) derived from Decitabine-induced ER-mediated enhancer-promoter interactions to stratify ER+ breast cancer patients in the METABRIC cohort into good and poor outcome groups. Data were analysed using the log-rank test. *P* values indicated within the graph. Distribution of the PAM50 classification in the high and low gene signature-expressing patients in the ER+ breast cancer METABRIC cohort.

(b) Kaplan–Meier survival plot showing ability of the gene signature identified in our study (n = 17 genes) derived from Decitabine-induced ER-mediated enhancer-promoter interactions to stratify ER+ breast cancer patients in the TCGA cohort into good and poor outcome groups. Data were analysed using the log-rank test. *P* values indicated within the graph. Distribution of the PAM50 classification in the high and low gene signature-expressing patients in the ER+ breast cancer TCGA cohort.

(c) Boxplot of normalised log2 gene expression levels of genes belonging to the signature in non-malignant (n = 145), poor outcome (n = 342) and good outcome (n = 832) ER+ breast tumours from the METABRIC cohort. *P* value Mann-Whitney t test.

(d) Boxplot of normalised log2 gene expression levels of genes belonging to the signature in poor outcome ("Dead", n = 109) and good outcome ("Alive", n = 568) ER+ breast tumours from the TCGA cohort. *P* value Mann-Whitney t test.

(e) Proposed model of tumour growth suppression induced by epigenetic therapy with Decitabine *via* DNA hypomethylation and subsequent re-wiring of ER-mediated enhancer-promoter interactions resulting in activation of specific ER target genes.

Extended Data Fig. 1

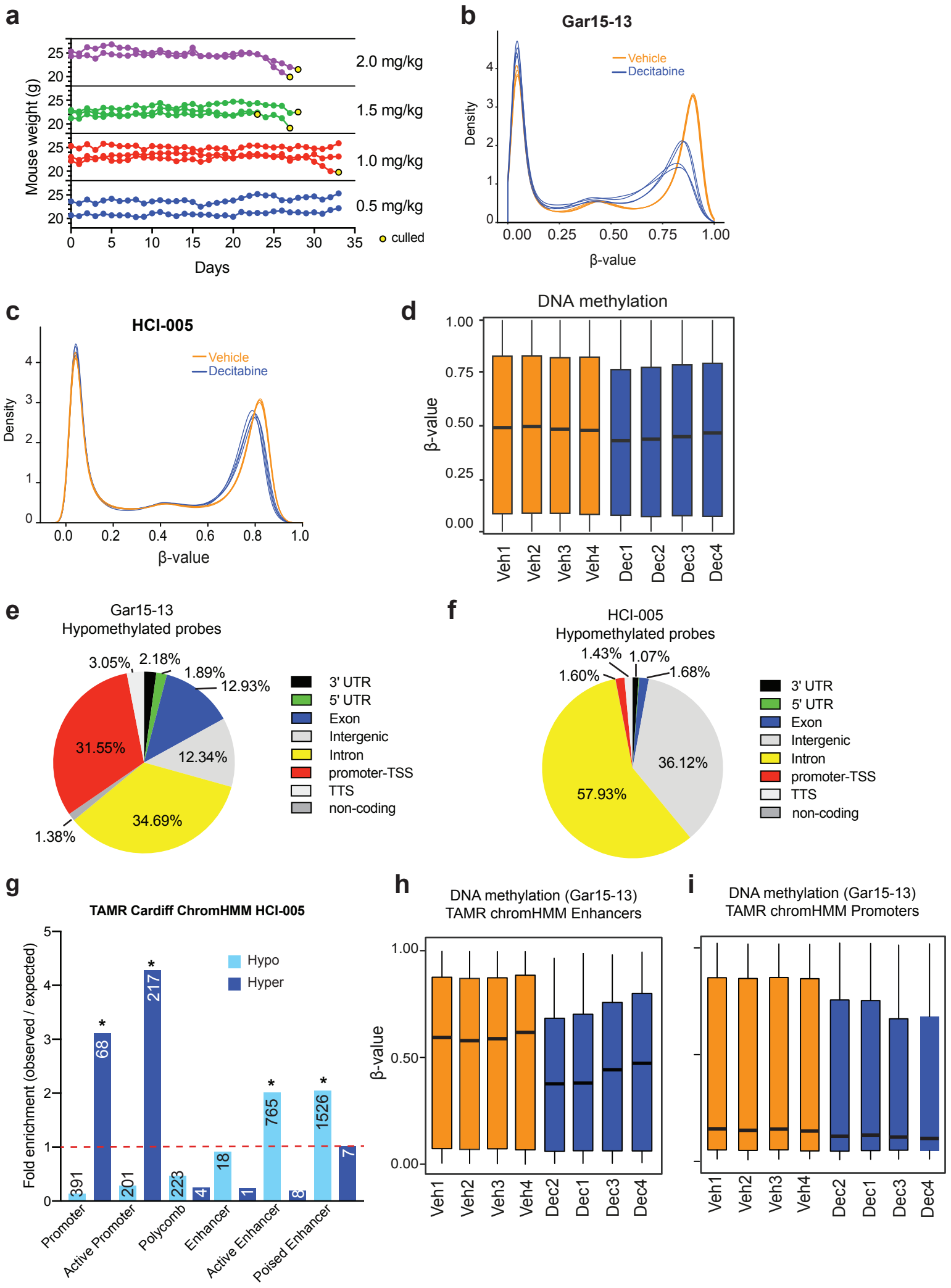

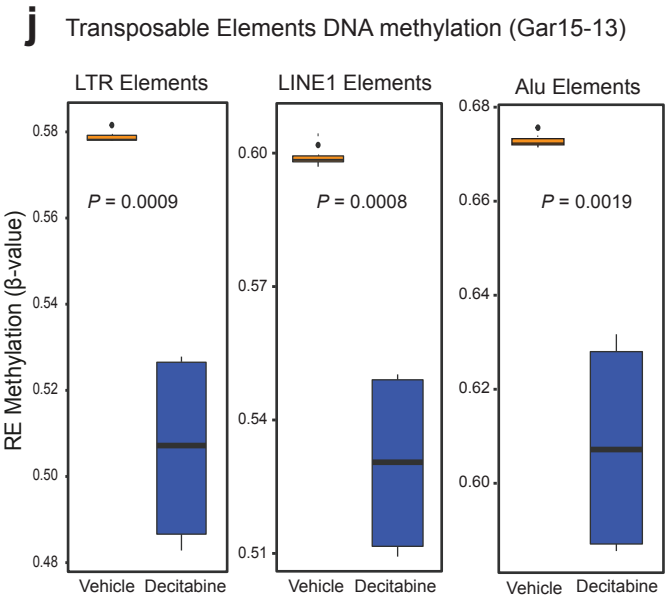
j
Transposable Elements DNA methylation (Gar15-13)
LTR Elements
LINE1 Elements
Alu Elements
RE Methylation (β-value)
P = 0.0009
P = 0.0008
P = 0.0019
Vehicle
Decitabine

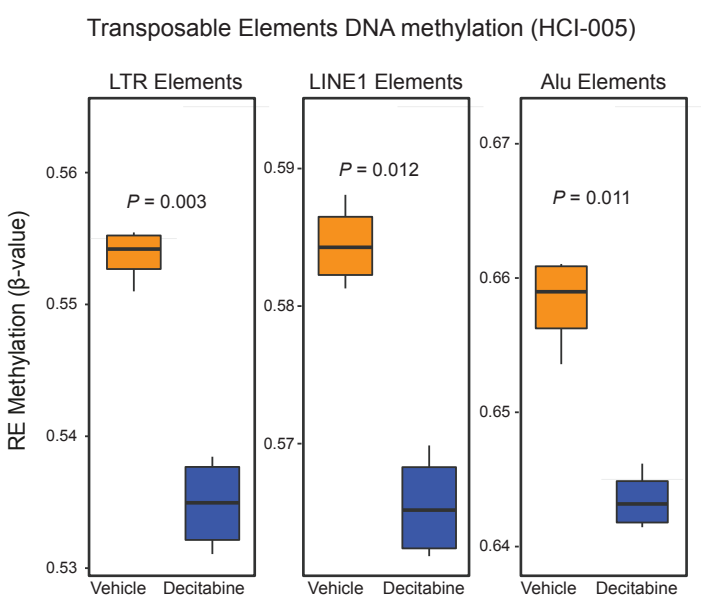
k
Transposable Elements DNA methylation (HCI-005)
LTR Elements
LINE1 Elements
Alu Elements
RE Methylation (β-value)
P = 0.003
P = 0.012
P = 0.011
Vehicle
Decitabine

Extended Data Fig. 1

(a) Mice were treated with indicated doses of Decitabine for 35 consecutive days and mice weight was assayed to determine the most appropriate Decitabine concentration.

(b) Density plot showing DNA methylation distribution in four Vehicle and four Decitabine-treated Gar15-13 tumours.

(c) Density plot showing DNA methylation distribution in four Vehicle and four Decitabine-treated HCI-005 tumours.

(d) Boxplots showing the distribution of DNA methylation profiles for HCI-005 Vehicle and Decitabine-treated tumours for all DNA methylation EPIC probes across the genome.

(e) RefSeq annotation of Vehicle vs. Decitabine hypomethylated probes (Gar15-13)

(f) RefSeq annotation of Vehicle vs. Decitabine hypomethylated probes (HCI-005)

(g) Bar plot showing the association of differentially methylated probes in HCI-005 Decitabine treatment compared to Vehicle across regulatory regions of the genome as determined by TAMR ChromHMM annotation. Observed over expected fold change enrichment shown. * P value < 0.001. The numbers of hypo/hypermethylated probes located within each specific regions are presented in the respective column.

(h) Boxplots showing the distribution of DNA methylation profiles for Gar15-13 Vehicle and Decitabine-treated tumours for EPIC probes located at TAMR ChromHMM enhancer regions. Black line indicates mean ± SD.

(i) Boxplots showing the distribution of DNA methylation profiles for Gar15-13 Vehicle and Decitabine-treated tumours for EPIC probes located at TAMR ChromHMM promoter regions. Black line indicates mean ± SD.

(j) Boxplots showing the distribution of DNA methylation for Gar15-13 Vehicle and Decitabine-treated tumours for EPIC probes mapping to LTR, LINE1 and Alu repetitive elements (REMP annotation). Black line indicates mean ± SD.

(k) Boxplots showing the distribution of DNA methylation profiles for HCI-005 Vehicle and Decitabine -treated tumours for EPIC probes mapping to LTR, LINE1 and Alu repetitive elements (REMP annotation). Black line indicates mean ± SD.

Extended Data Fig. 2

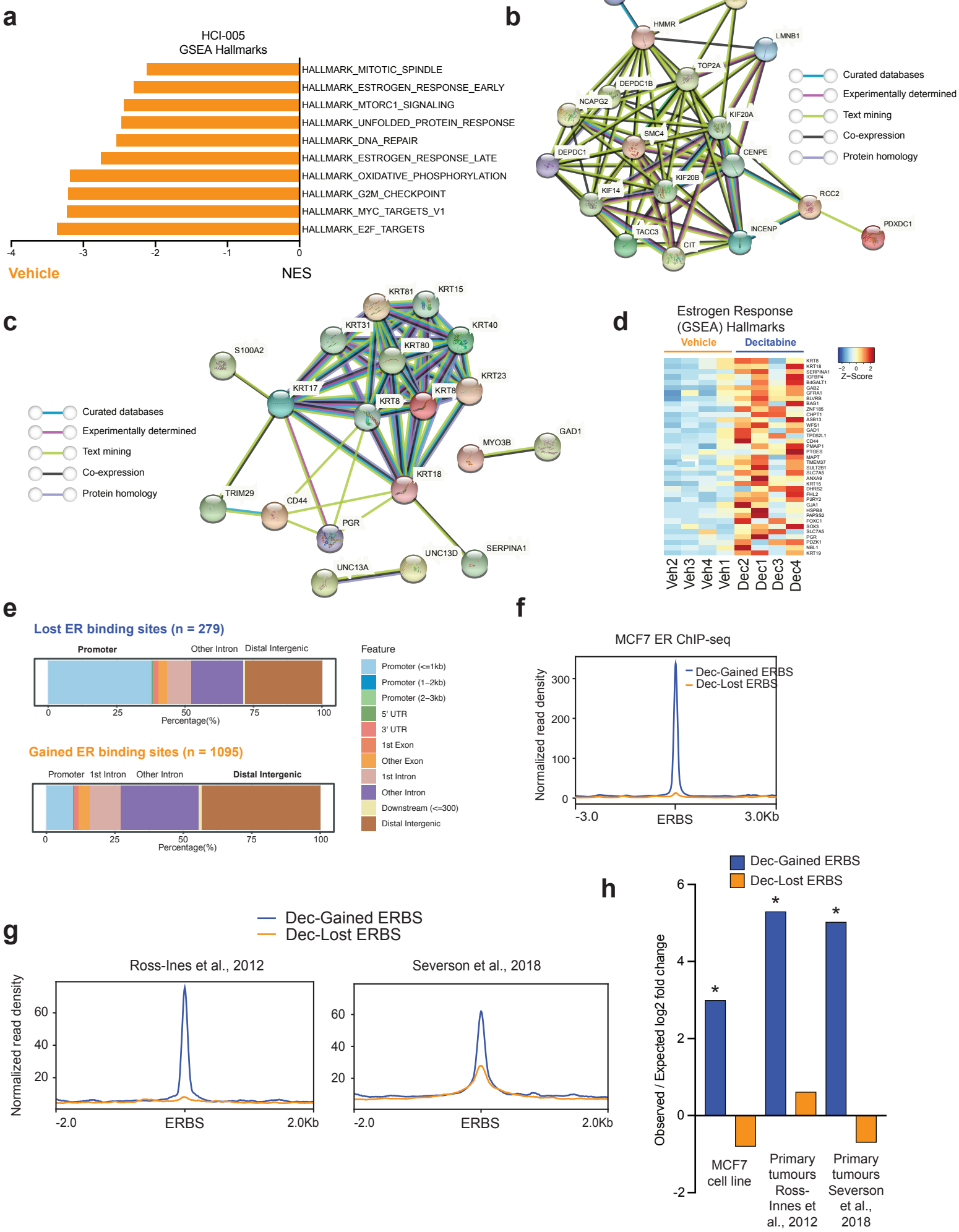

i

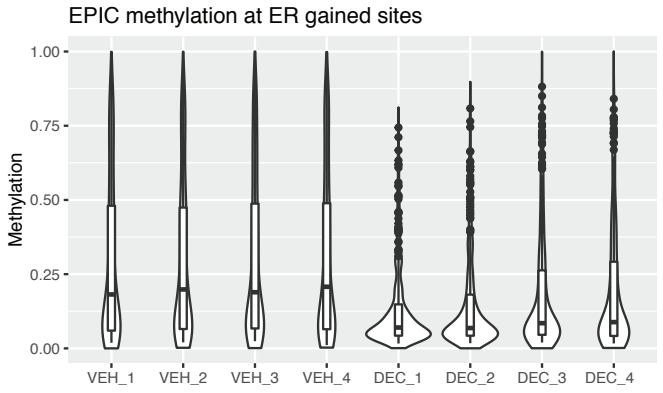
EPIC methylation at ER gained sites
Methylation
1.00
0.75
0.50
0.25
0.00
VEH_1
VEH_2
VEH_3
VEH_4
DEC_1
DEC_2
DEC_3
DEC_4

j

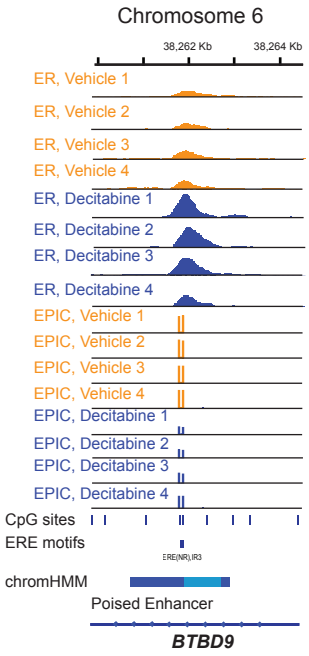
Chromosome 6
38,262 Kb
38,264 Kb
ER, Vehicle 1
ER, Vehicle 2
ER, Vehicle 3
ER, Vehicle 4
ER, Decitabine 1
ER, Decitabine 2
ER, Decitabine 3
ER, Decitabine 4
EPIC, Vehicle 1
EPIC, Vehicle 2
EPIC, Vehicle 3
EPIC, Vehicle 4
EPIC, Decitabine 1
EPIC, Decitabine 2
EPIC, Decitabine 3
EPIC, Decitabine 4
CpG sites
ERE motifs
chromHMM
Poised Enhancer
BTBD9

k

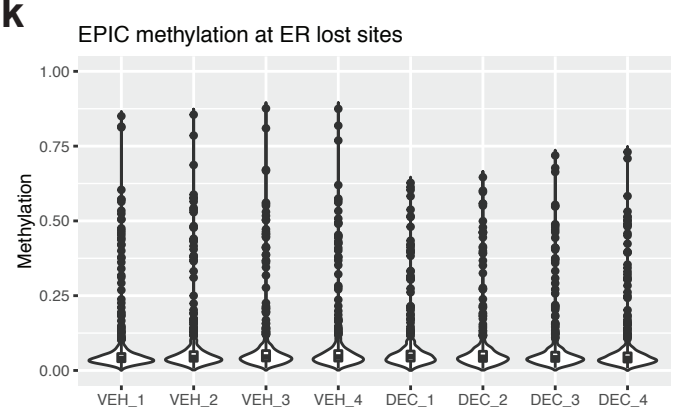
EPIC methylation at ER lost sites
Methylation
1.00
0.75
0.50
0.25
0.00
VEH_1
VEH_2
VEH_3
VEH_4
DEC_1
DEC_2
DEC_3
DEC_4

Extended Data Fig. 2

(a) Normalized enrichment scores (NES) for signature gene sets representing differentially expressed genes in RNA-seq data from HCI-005 PDX tumours treated with Decitabine compared to Vehicle (n = 4; hallmarks with FDR < 0.05 are shown)

(b) Protein-protein interaction analyses of down-regulated genes belonging to the E2F Targets and G2M Checkpoint (GSEA) Hallmark. Interaction confidence indicated on the graph.

(c) Protein-protein interaction analyses of up-regulated genes belonging to the Estrogen Response (GSEA) Hallmark. Interaction confidence indicated on the graph.

(d) RNA-seq heatmap of Decitabine-induced changes in expression of genes belonging to the Estrogen Response (GSEA) Hallmarks. Top differentially expressed genes plotted (FDR < 0.05).

(e) RefSeq annotation of Vehicle vs. Decitabine lost and gained ER binding sites in Gar15-13.

(f) Average signal intensity of MCF7 ER ChIP-seq binding at ER binding sites gained and lost with Decitabine treatment. Merged data from n = 3 replicates shown.

(g) Average signal intensity of ER ChIP-seq binding in primary ER+ breast tumours from patients at ER binding sites gained and lost with Decitabine treatment. ChIP-seq data obtained from Ross-Innes et al., 2012 (left panel) and Severson et al., 2018 (right panel). Merged data from n = 9 (left panel) and n = 6 (right panel) shown.

(h) Observed/expected log2 enrichment of consensus ER binding sites in MCF7 cell line and primary ER+ breast tumours from Ross-Innes et al., 2012 and Severson et al., 2018 at ER binding sites gained and lost with Decitabine treatment. * *P* value < 0.001; permutation test.

(i) Violin plot showing DNA methylation levels at gained ER binding sites in Decitabine-treated (n = 4) and Vehicle (n = 4) PDX Gar15-13 tumours.

(j) Browser snapshot of ER ChIP-seq and EPIC DNA methylation (Vehicle and Decitabine-treated tumours, n = 4 each), showing concomitant gain of ER binding and loss of DNA methylation at enhancer of ER target gene *BTBD9*.

(k) Violin plot showing DNA methylation levels at lost ER binding sites in Decitabine-treated (n = 4) and Vehicle (n = 4) Gar15-13 tumours.

Extended Data Fig. 3

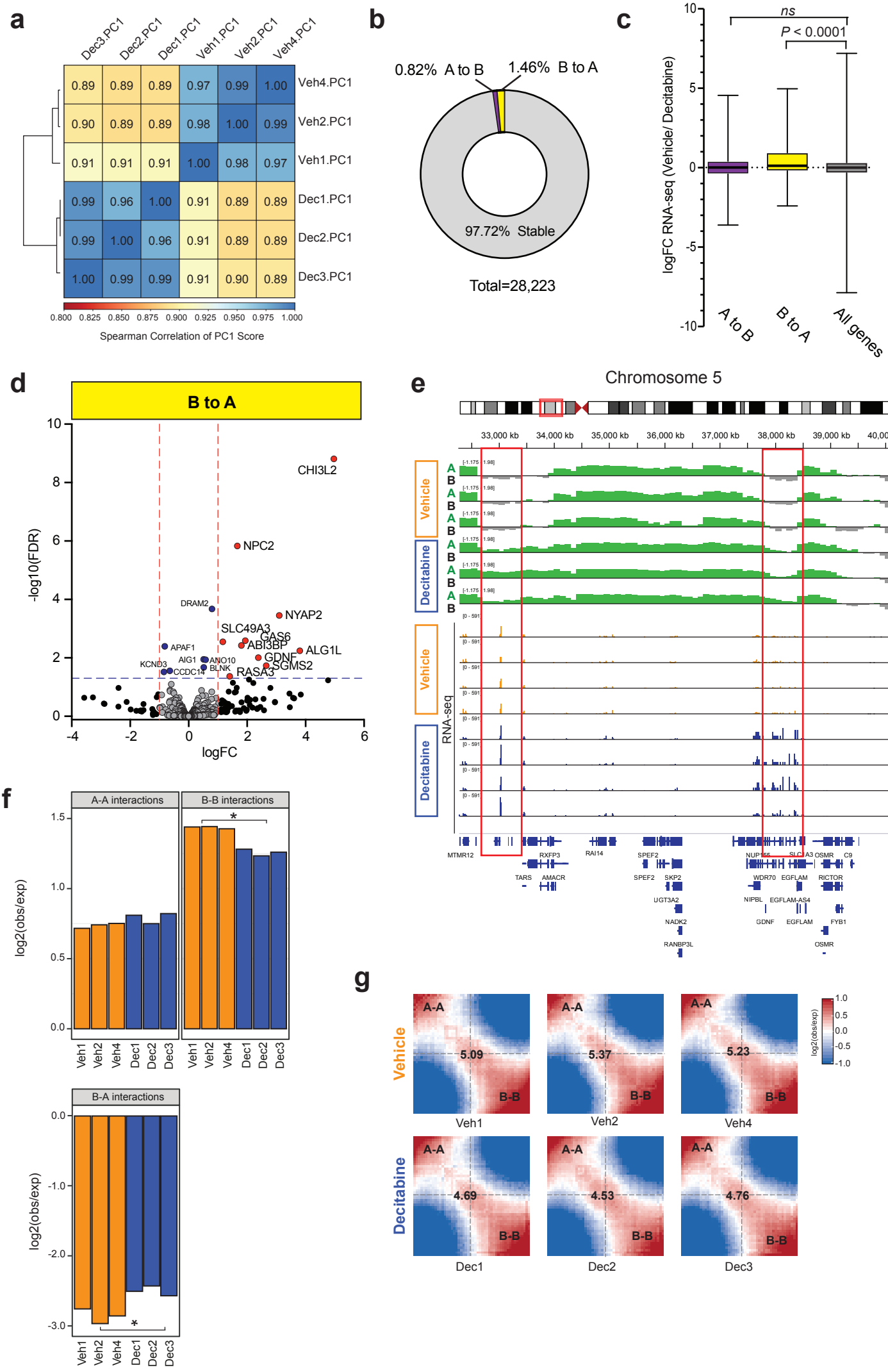

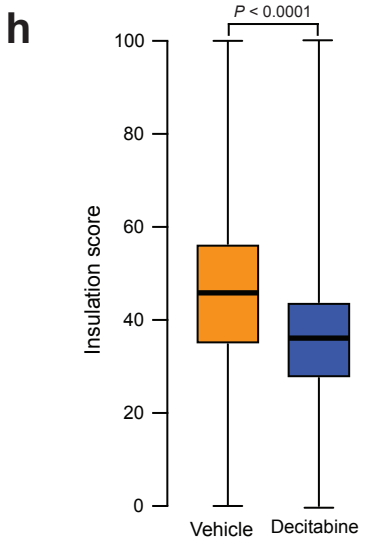
h
P < 0.0001
Insulation score
100
80
60
40
20
0
Vehicle
Decitabine

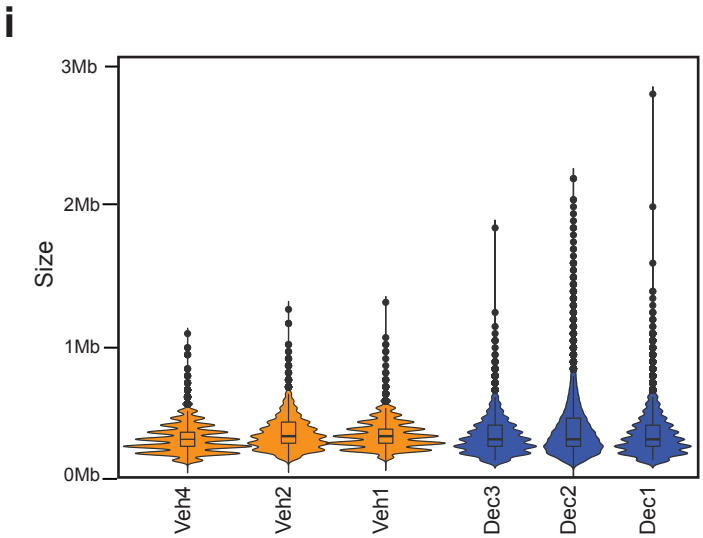
i
Size
3Mb
2Mb
1Mb
0Mb
Veh4
Veh2
Veh1
Dec3
Dec2
Dec1

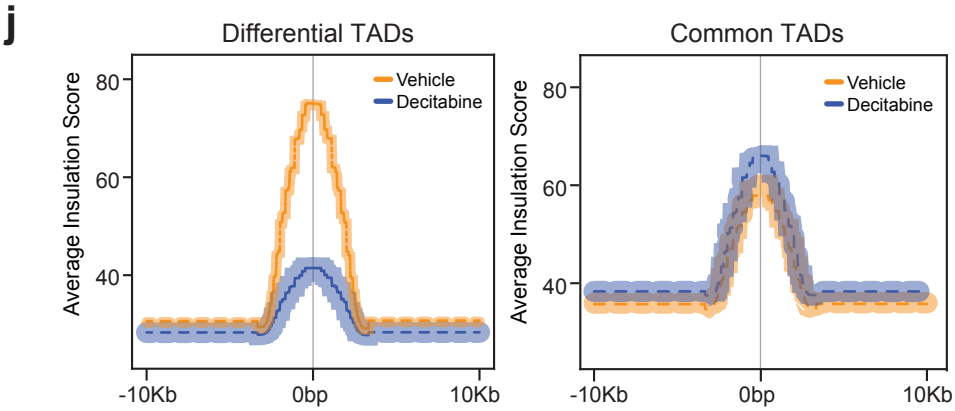
j
Differential TADs
Common TADs
Average Insulation Score
80
60
40
Vehicle
Decitabine
-10Kb
0bp
10Kb

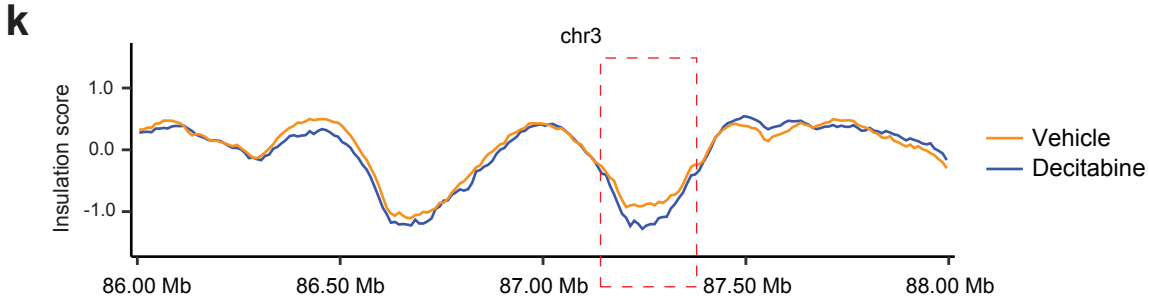
k
chr3
Insulation score
1.0
0.0
-1.0
86.00 Mb
86.50 Mb
87.00 Mb
87.50 Mb
88.00 Mb
Vehicle
Decitabine

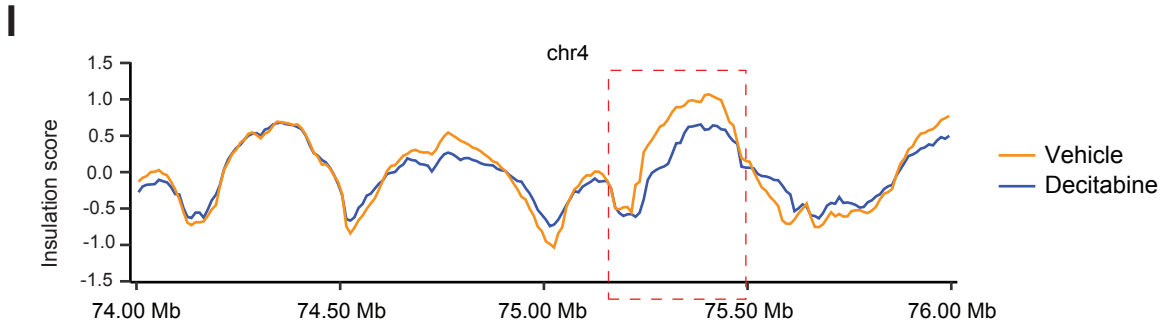
l
chr4
Insulation score
1.5
1.0
0.5
0.0
-0.5
-1.0
-1.5
74.00 Mb
74.50 Mb
75.00 Mb
75.50 Mb
76.00 Mb
Vehicle
Decitabine

Extended Data Fig. 3

(a) Heatmap showing Spearman pairwise correlations between the eigenvectors (PC1) in three Decitabine-treated and three Vehicle PDX Gar15-13 tumours. Samples are ordered according to complete linkage hierarchal clustering.

(b) Pie chart showing distributing of stable (A to A; B to B) and switching (A to B; B to A) compartments in Decitabine-treated tumours compared to Vehicle

(c) Barplot showing logFC expression between Vehicle and Decitabine-treated tumours of genes located either at A to B or B to A switching compartments. *P* value: Wilcox rank-sum test.

(d) Volcano plot showing Decitabine *vs.* Vehicle differential expression of genes located at compartment that switched from B to A assignment in Decitabine-treated tumours.

(e) Browser snapshot of Hi-C eigenvectors and RNA-seq in Vehicle and Decitabine-treated tumours (n = 3 Hi-C and n = 4 RNA-seq each), showing demarcation of open (A-type; positive values) and closed (B-type; negative values) compartment changes across a region on chromosome 5, which is associated with increased expression of genes located within this region.

(f) Barplot showing log2 observed over expected A – A, B – B and B – A compartment interactions in Vehicle and Decitabine tumours. * *P* value two-tailed Students t-test < 0.05

(**g**) Average contact enrichment between pairs of 50Kb loci arranged by their PC1 eigenvector in Vehicle and Decitabine-treated tumours. The numbers at the center of the heatmaps indicate compartment strength calculated as the log2 ratio of (A–A + B–B)/ (A–B + B–A) using the mean values.

(h) Boxplot of average insulation score calculated by TADtool at 50Kb resolution in three replicates of Decitabine-treated and Vehicle PDX tumours. *P* value Wilcox rank-sum test.

(i) Violin plot showing the distribution in TAD sizes for Vehicle and Decitabine treated Gar15-13 tumours (n = 3 each).

(j) Average insulation score at differential and common TADs. Lines show mean values, while light shading represents SEM.

(k) Snapshot of region on chromosome 3, showing insulation score calculated in Vehicle and Decitabine-treated tumour Hi-C matrixes, demonstrating loss of TAD

boundary insulation is Decitabine-treated samples (indicated with a red box). Merged Hi-C data from replicates shown at 10Kb resolution.

(l) Snapshot of region on chromosome 4, showing insulation score calculated in Vehicle and Decitabine-treated tumour Hi-C matrixes, demonstrating loss of TAD boundary insulation is Decitabine-treated samples (indicated with a red box). Merged Hi-C data from replicates shown at 10Kb resolution.

Extended Data Fig. 4

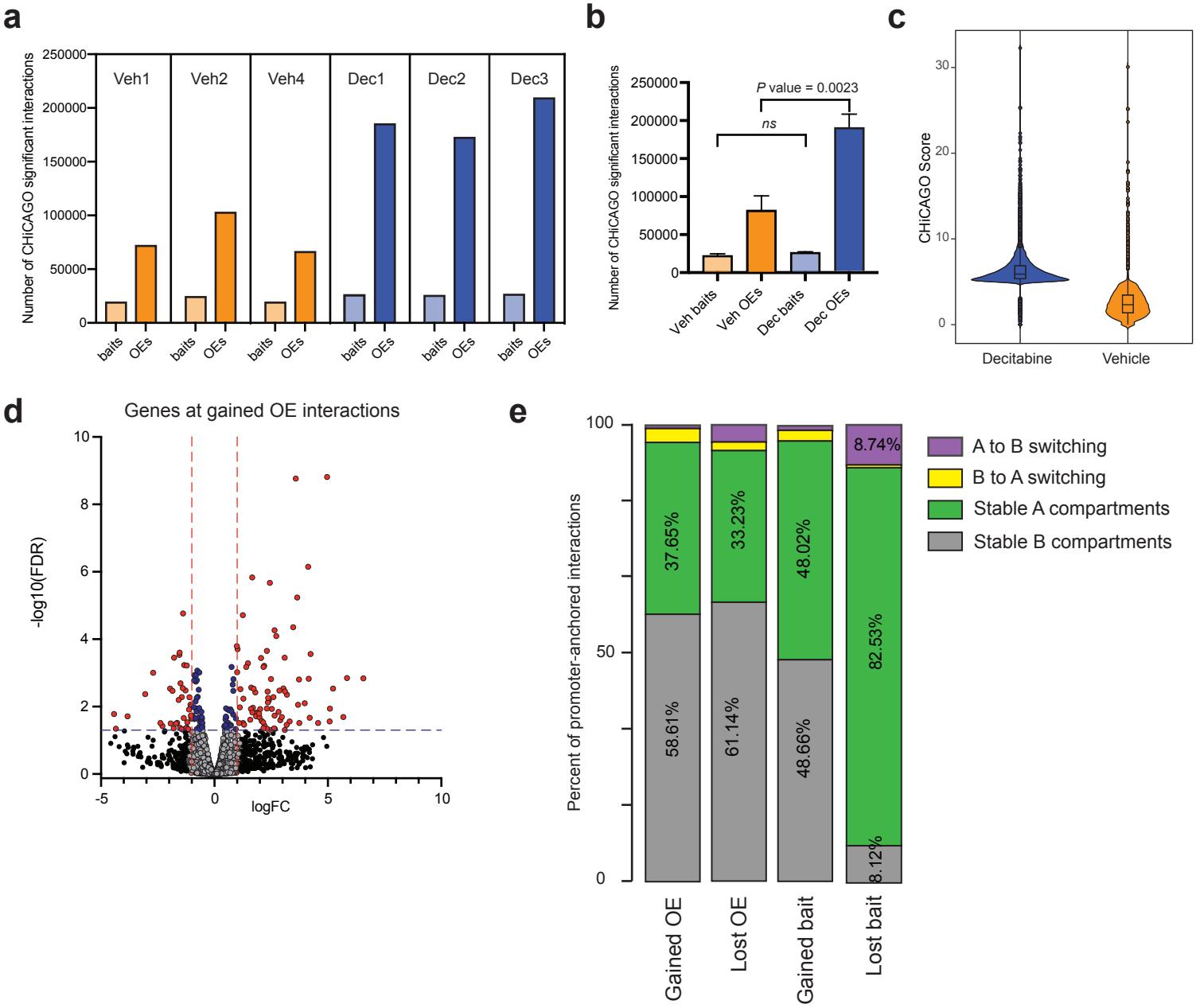

Extended Data Fig. 4

(a) Number of promoter baits and enhancer OEs involved in significant CHiCAGO interactions for each of the PCHi-C maps from Vehicle and Decitabine-treated Gar15-13 tumours (n = 3 each).

(b) Average number of promoter baits and enhancer OEs involved in significant CHiCAGO interactions across the three Vehicle and three Decitabine-treated PCHi-C replicates. Error bars indicate SD. *P* value Wilcoxon rank-sum test.

(c) Boxplot of ChICAGO scores of promoter-anchored interactions identified from PCHi-C data in Decitabine and Vehicle tumours. Data from n = 3 tumours shown.

(d) Volcano plot showing Decitabine *vs.* Vehicle differential expression of genes that are located at enhancer-promoter interactions gained with Decitabine treatment.

(e) Bar plot showing the percentage of promoter-anchored interactions located in chromosomal compartments that switched assignments (A to B or B to A) and stable A or B compartments.

Extended Data Fig. 5

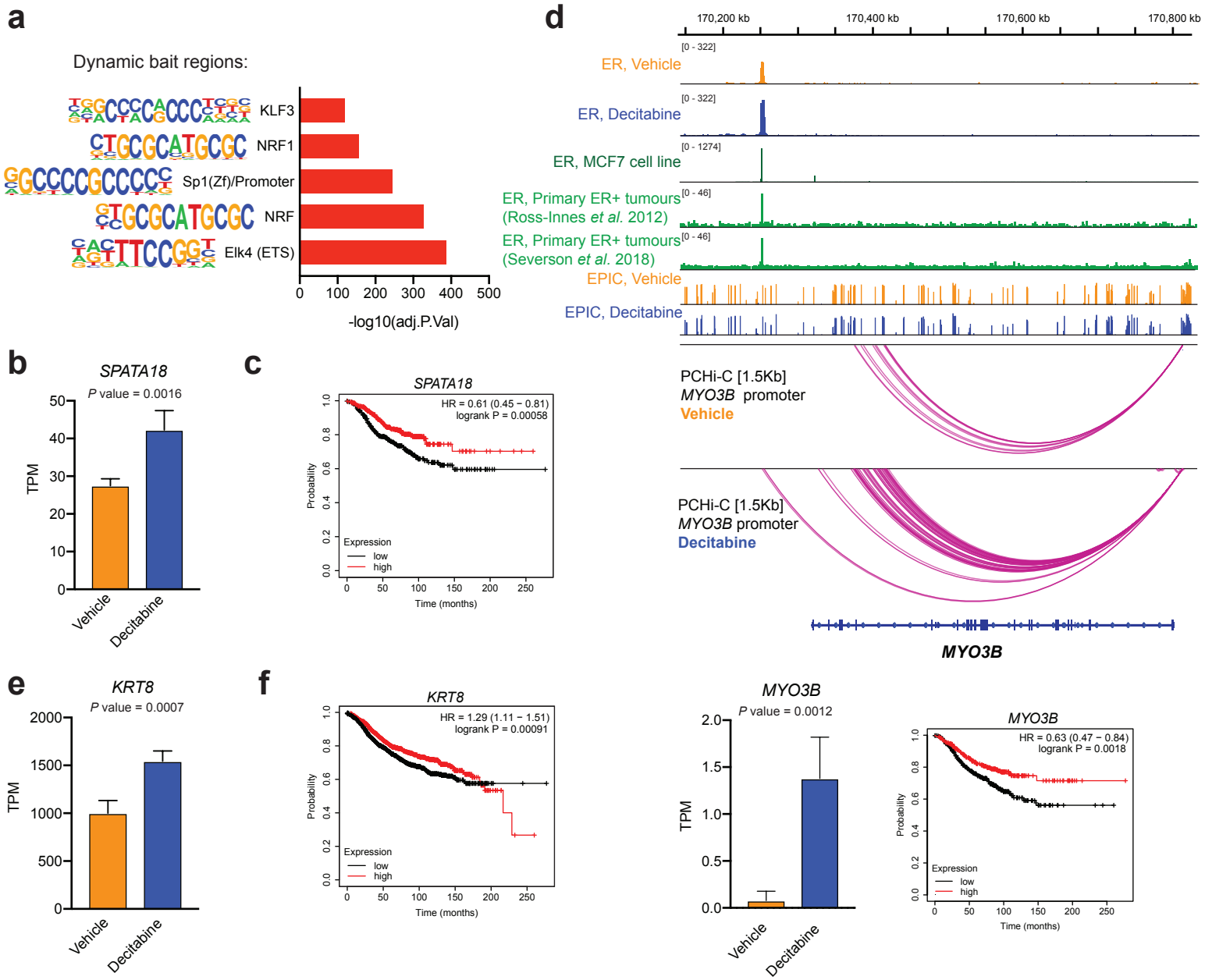

Extended Data Fig. 5

(a) Transcription factor binding motifs enriched at promoter-anchored interactions involving dynamic promoter bait regions. Only motifs with FDR < 0.05 shown.

(b) The relative mRNA expression levels of *SPATA18* gene from RNA-seq (two-tailed t-test $P < 0.05$ derived from four replicates). Error bars indicate standard deviation from four samples.

(c) Kaplan–Meier survival plot showing the ability of *SPATA18* gene to stratify ER+ breast cancer patients in the METABRIC cohort into good and poor outcome groups. Data were analysed using the log-rank test. *P* values indicated within the graph.

(d) Browser snapshots showing the promoter-anchored interactions at the *MYO3B* ER target gene, together with ER ChIP-seq, EPIC DNA methylation and ChromHMM track. Merged replicate data shown (n = 4 each). In Decitabine-treated tumours, the *MYO3B* promoter displays increased number of interactions with an enhancer, which gains ER binding with Decitabine treatment. This gained ER binding site is also present in ER ChIP-seq data from primary ER+ breast tumours from Ross-Innes *et al.,* 2012 and Severson *et al.,* 2018. The relative expression of the *MYO3B* gene was significantly upregulated in Decitabine-treated tumours (two-tailed t-test $P < 0.05$ derived from four replicates) and associated with good outcome in ER+ breast cancer patients in the METABRIC cohort. Data were analysed using the log-rank test. *P* values indicated within the graph.

(e) The relative mRNA expression levels of *KRT8* gene from RNA-seq (two-tailed t-test $P < 0.05$ derived from four replicates). Error bars indicate standard deviation from four samples.

(f) Kaplan–Meier survival plot showing the ability of *KRT8* gene to stratify ER+ breast cancer patients in the METABRIC cohort into good and poor outcome groups. Data were analysed using the log-rank test. *P* values indicated within the graph.